WORKSPACE OPTIMIZATION OF A SIX DEGREE OF FREEDOM PARALLEL MANIPULATOR FOR MICROMACHINING

by

Ahmet Ağaoğlu

Submitted to the Institute of Graduate Studies in

Science and Engineering in partial fulfillment of

the requirements for the degree of

Master of Science

in

Mechanical Engineering

Yeditepe University

2010

WORKSPACE OPTIMIZATION OF A SIX DEGREE OF FREEDOM PARALLEL MANIPULATOR FOR MICROMACHINING

APPROVED BY:

Assist. Prof. Namık Çıblak (Supervisor) ....

Assist. Prof. Koray K. Şafak ....

Assoc. Prof. Korkut Yeğin ....

ACKNOWLEDGEMENTS

I would like to express my appreciation to my instructors: Dr. Namık Çıblak and Dr. Koray K. Şafak. Thanks for giving me the opportunity to be part of the Yeditepe Parallel Manipulator Project. Special thanks to Dr. Çıblak for his time, patience, and understanding. Dr. Çıblak, it has been an honor to work with you. Also, thanks to TUBITAK for making this study possible by providing funding to me and Yeditepe University (Project No: 105M213).

I dedicate this thesis to my parents who unremittingly supported me during my years of education. They made this work possible.

The most special thank goes to my best partner and friend, Şuda Ayşe Karaduman. Şuda, you gave me your unconditional support and encouraged me through all this long process.

ABSTRACT

WORKSPACE OPTIMIZATION OF A SIX DEGREE OF FREEDOM PARALLEL MANIPULATOR FOR MICROMACHINING

This work addresses the optimization of the workspace of a six degree of freedom parallel manipulator. In this study, topology of the manipulator is composed of three xy-tables, symmetrically positioned on a circle on a base plane, connected by three legs to a moving platform. Kinematic composition of the manipulator is introduced and kinematic diagram is illustrated. Orientation workspace is investigated using three different orientation representations. XYZ fixed angles representation is selected upon the benefits of its visualization are considered. By using this representation, the orientation workspace is modeled and kinematic circuits of the manipulator are explored. First, optimization is performed without slider limitations. A result table is obtained based on the user defined parameters. Secondly, optimization is performed under slider limitations. The maximal orientation capability is optimized using numerical analysis. The optimized configuration of the manipulator indicates that a 330% increase in orientation capability, compared to the old configuration.

ÖZET

ALTI SERBESTLİK DERECELİ MİKRO İŞLEME İÇİN ÜRETİLEN PARALEL BİR ROBOTUN ÇALIŞMA UZAYI OPTİMİZASYONU

Bu çalışmada, altı serbestlik derecesine sahip paralel bir robotun, çalışma uzayı optimizasyonu yapılmıştır. Bu çalışmada kullanılan robotun yapısı, taban düzlemi üzerine simetrik olarak yerleştirilen üç xy kızağının, üç özdeş bacakla hareketli bir platforma bağlanması şeklinde tanımlanabilir. Robotun kinematik kompozisyonu tanıtılmış ve kinematik diyagramı gösterilmiştir. Oryantasyon çalışma uzayı üç farklı metotla incelenmiştir. XYZ Euler açıları, çalışma uzayının görüntülenmesi aşamasında sağladığı avantajlarla, bu metotlar arasında en uygunu olarak belirlenmiştir. Bu metot kullanılarak oryantasyon çalışma uzayı modellenmiş ve robotun kinematik çevrimleri keşfedilmiştir. İlk optimizasyon, kızak limitleri düşünülmeden gerçekleştirilmiştir. Bu çalışmaya göre, kullanıcı tanımlı bir sonuç tablosu elde edilmiştir. İkinci optimizasyonda ise kızak limitleri işlemlere katılmış ve maksimum oryantasyon yeteneğinin en iyi değeri, sayısal analiz kullanılarak hesaplanmıştır. Eski konfigürasyona göre 330%’ lük bir artış sağlanmıştır.

TABLE OF CONTENTS

LIST OF FIGURES

LIST OF TABLES

LIST OF SYMBOLS / ABBREVIATIONS

L	Leg length
$L_{critical}$	Critical leg length
O_B	Origin of the base frame
O_P	Origin of the platform frame
P	Platform position vector
R_B	Radius of the base circle
R_i	Specific rotation matrix about platform z axis
R_p	Platform rotation matrix
R_{Si}	Specific rotation matrix about base z axis
R_{sphere}	Radius of the workspace sphere
S_i	Slider position vector
s_x, s_y, s_z	Rodrigues Parameters
S	Skew symmetric matrix
u	Rotation axis
α	Azimuth angle
α	Rotation about z axis
β	Elevation angle
β	Rotation about y axis
γ	Rotation about x axis
Δz	Operational height
θ	Rotation amount
θ_i	Leg angle
ρ	Radius of the platform circle
YPM	Yeditepe parallel manipulator

1. INTRODUCTION

As demands for micro parts are on the increase in such industries as aerospace, biomedical, electronics, environment, information technology, and displays, the need for manufacturing such parts is also increasing. It is widely accepted that the development of precision manufacturing has greatly changed our lives in terms of increased living standards. High precision manufacturing offers quality and reliability for conventional products, but also makes possible entirely new products, especially where mechatronics, miniaturization, and high performance are important. Impressive examples are digital cameras, mobile phones, minimal invasive medical equipment, as well as biotechnological or chemical processing equipment. The high function density and reduced size and weight will make the miniature and micro products more competitive. As a result, the markets for miniature and micro components hold a high potential of growth.

Recently new demands in the fabrication of miniature/microproducts have appeared such as manufacturing of microstructures and components with 3D complex shapes or free-form surfaces. Some of these microstructures have some special functions including light guiding, anti-reflecting and self-cleaning and so on. The microstructures will further improve the performance of miniature and micro products. Furthermore, fabrication of real 3D miniaturized structures and free-form surfaces are also driven by the integration of multiple functions in one product.

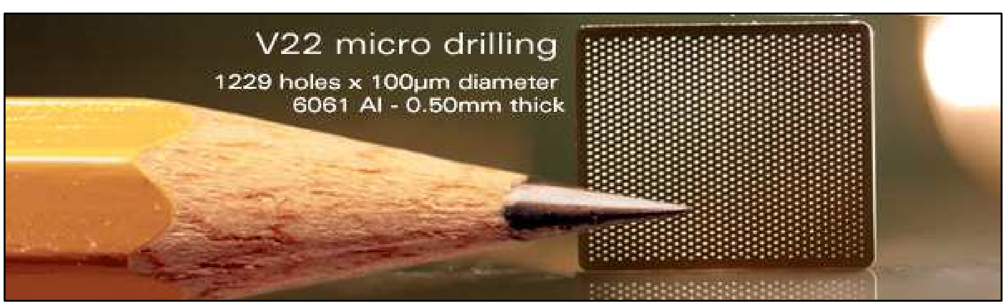

Figure 1.1. An example of micro drilled component [1]

Currently MEMS is one of the major driving forces for making micro-components. Silicon is a classic material for MEMS or microsystems, but many other materials have appeared for the increasing number of applications which are becoming relevant for micro products. For example, the life sciences, as developing application areas of MEMS require glass, ceramics, metal and plastics rather than only silicon as raw materials of micro components.

Major methods of manufacturing micro parts are based on non-traditional machining, such as lithography, etching, lasers, ultrasonic, ion-beam and electrical discharge. However, the material removal rate of these methods is relatively slow, and workpiece materials and applicable shapes are limited. Therefore, mechanical machining is required for the manufacturing of micro parts with complex shapes. The end milling process can be applied to the manufacturing of a variety of shapes from macro to micro scale levels. This process can cost-effectively produce micro parts because equipment costs are relatively low compared with other processes.

Although traditional mechanical ultraprecision machining has been used as a major means to fabricate miniature and micro components, it still remains a big issue in the predictability, producibility and productivity of fabrication of microproducts, especially for those miniature and micro components with complex surface forms. The ultraprecision machine tools design and machining technology will have to be changed so as to achieve a rapid and economic fabrication of those components and products in a variety of engineering materials and ensure that the machines and technology are easily accessible to the wider audience of precision engineering.

Parallel manipulators are widely accepted as ideal candidates for use in manufacturing industries for their superior properties compared to serial manipulators, such as low inertia, high stiffness, and high precision. However, relatively small workspace, complex input-output relationship, and lots of singularities in their workspaces cancel out the mentioned advantages. Choosing a set of geometric parameters so as to achieve desired/optimal performance and reducing these disadvantages has a vital significance in robotics research.

Among all kinematic measures, workspace is the most important index in the design of a parallel manipulator. In regard to workspace requirements, there are two types of formulations of the design problem. One is to generate a manipulator whose workspace contains a prescribed workspace. The other possible formulation is to find the geometry of a parallel manipulator that maximizes workspace. A parallel manipulator designed only for maximum workspace may not be a good design in practice. It is possible that the manipulator with maximum workspace has undesirable kinematic characteristics such as poor orientation capability.

In this manner, a high precision parallel manipulator for micromachining of free form surfaces has been under development since 2006 by Ciblak and Safak. This project is in collaboration with Koc University and funded by TUBITAK (Project No: 105M213. 1/11/2006 -1/11/2009). This study aims to optimize the workspace of Yeditepe Parallel Manipulator (YPM), especially the orientation capability.

This dissertation is organized as follows. In chapter 2, a comprehensive literature survey is presented. The literature survey is classified as the optimization of the parallel manipulators considering accuracy, stiffness, and workspace. In this manner various parallel kinematic structures are introduced and optimization results are highlighted.

In chapter 3, topology of the YPM is studied. In order to investigate the topology, kinematic composition is listed and the mechanical components are introduced. Physical constraints of kinematic structure are explored. The kinematic diagram is illustrated.

In chapter 4, kinematics of the YPM is considered. Inverse kinematic solution is examined and the kinematic structure of the YPM is investigated.

In chapter 5, definition of the workspace is stated. Concept of translational and orientation workspace is reviewed. Orientation workspace is represented with three different methods and one of them is selected according to visualization quality. The orientation workspace is plotted by various representations. In addition to this, the orientation workspace is discussed in detail and the features of the orientation workspace are investigated.

In chapter 6, optimization of the workspace is performed. In the first section, the optimization is considered with no slider limitations. Optimum dimensional configurations are enlightened according to application type. In the second part, optimization is considered with slider limitations. An optimum result is found and it is shown that a 330% improvement is achieved.

2. LITERATURE SURVEY

In the future, the precision manipulation of small objects will become more and more important for appliances such as (probe-based) data storage, micro-assembly, sample manipulation in microscopes, cell manipulation, nano-indenting, manipulation of optical beam paths by micro-mirrors and manipulation of electron beam paths by phase plates and especially for micromachining of small objects.

The major potential in precision manipulation can be found in fabrication of Micro Mechanical Systems. Most fabrication methods are based on the lithography process, which enables design of 2-dimensional shapes by layer etching and deposition. Consequently, components of the micro-mechanisms usually have a planar geometry, and it is hard to manufacture components that have free form surfaces.

While in the macro world the decision which robot type to use, either serial or parallel, is based on the specific application, in the micro world there is a clearer conclusion that parallel manipulator structures are more suitable for micro components fabrication technology [2]. Therefore the design optimization of the parallel manipulators should be studied to manufacture dexterous parallel manipulators.

Optimization methodologies have long been applied to mechanism synthesis [3]. Optimization of robot manipulators is a natural extension of this idea to multi-degree-of-freedom (DOF) mechanisms. Mechanisms have traditionally been single-DOF systems designed to perform only one specific task, and so the design objective was typically a measure of the mechanism’s ability to follow a specific trajectory or to generate a specified force/torque as a function of time. The main idea of robotics is to realize computer controlled multi-DOF mechanisms which can readily perform a wide range of tasks. Thus, at the design stage, the objective function for optimizing a robotic mechanism must differ significantly from that of a single-DOF mechanism. A number of different optimization criteria for robot manipulators may be appropriate depending on the resources available and the general nature of tasks to be performed. For example, if computational resources are limited, then simplicity of the kinematic relationships is important. If robots must repair themselves in a remote environment (such as a space station), then simplicity and ease of assembly become important; and if obstacles must be avoided, then redundancy and elimination of singularities take precedence. When the objective criterion is chosen as the workspace volume by defining a “well-connected workspace,” then elbow-type serial link manipulators are optimal. A redundant 7-DOF serial link manipulator was shown to be the best fit to a number of different objective criteria which included elimination of singularities, simplicity of analysis, ease of construction, and workspace shape [4]. Other criteria may include accuracy (static and dynamic), load capacity, speed, and robustness.

The parallel manipulator performances are highly sensitive to the kinematic configuration of the mechanism. However, adjusting the geometry of a parallel manipulator so that it is "optimal" with respect to a given task is a difficult problem. It can be considered as three main criteria for optimality:

- The first criterion is the accuracy criterion where the accuracy of the robot plays a big role.
- The second criterion may be considered for operational performance. In this manner, stiffness optimization is proposed to resist to dynamic and external forces with small deflections. For an optimal control, optimality index can also be considered as the minimal stiffness of the robot along a given trajectory. In that case a method to determine an optimal geometry that increases the performance of the robot may be obtained.
- Finally, optimal workspace criterion may be considered. The studies in the literature can be classified according to these three criteria.

These are respectively presented in what follows.

2.1. ACCURACY CRITERION

A prescribed degree of freedom parallel robot that has to move within a given workspace and whose geometry is defined by a set of parameters is considered in [5]. The motions of active joints of the manipulator are measured with sensors with a known accuracy $\pm\Delta\rho$. These errors together with bounded manufacturing errors on the parameters describing the geometry of the robot induce a positioning error of the platform.

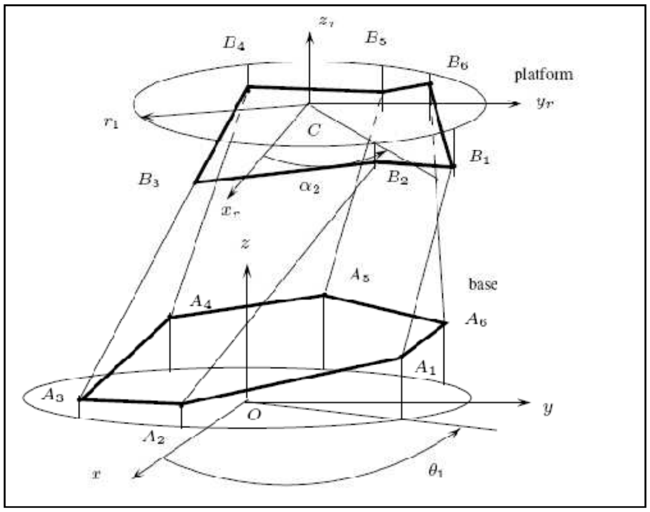

Figure 2.1. The geometrical parameters of the robot [5]

The desired vector of maximal positioning errors is expressed by the Jacobian of the robot and ρ, in an analytic form using the generalized parameters. Therefore using linear algebra, the Jacobian matrix is represented in a form of maximum position errors and accuracy constraints. An algorithm that allows one to determine geometries of the robot ensuring that these positioning errors will lie within pre-specified limits is developed. Another benefit of this algorithm is also the computation of the maximal positioning errors of a given robot up to a predefined accuracy [5].

Ng, Ong and, Nee presented research and development of a three–legged micro parallel kinematic manipulator for positioning in micromachining and assembly operations under the consideration of accuracy by using a numerical approach [6]. In that paper, the structural characteristics associated with different kinds of parallel manipulators are evaluated using MATLAB, and, the translational and rotational movements of the manipulators are identified to decide a suitable parallel kinematics model, (Figure 2.2).

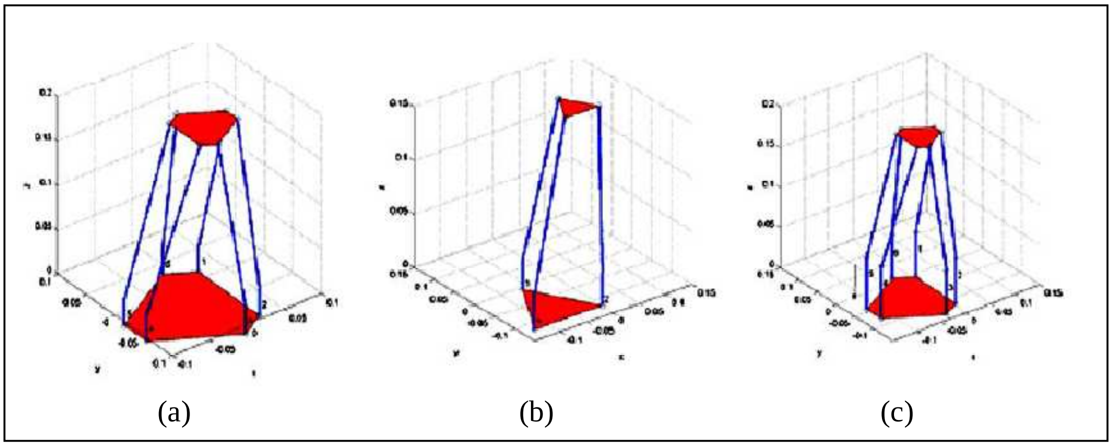

Figure 2.2. (a) six-legged micro Stewart platform, (b) three-legged micro Stewart platform, (c) PSU micro Stewart platform [6]

Based on these identifications, a hybrid 3–UPU (universal joint–prismatic joint–universal joint) parallel manipulator is designed and fabricated. The principles of the operation and modeling of this micro PKM are largely similar to a normal-sized Stewart platform. The overall size of the platform is contained within a space of 300 mm×300 mm×300 mm. A modular design methodology is introduced for the construction of this micro PKM. Calibration results in addition to position and orientation errors of this hybrid 3–UPU PKM are also discussed.

Another phenomenon in consideration of robot accuracy is the analysis of condition number. In fact, the condition number of a matrix is used in numerical analysis to estimate the error generated in the solution of a linear system of equations by the error on the data. When applied to the Jacobian matrix, the condition number gives a measure of the accuracy of the Cartesian velocity of the end effector and the static load acting on the end effector.

An example of this is studied in [7] to optimize the operation performance of the manipulators. In this study in addition to the conditioning index, stiffness of the robot is also considered to select the link lengths of 3-DOF spherical parallel manipulators to analyze their operational performance.

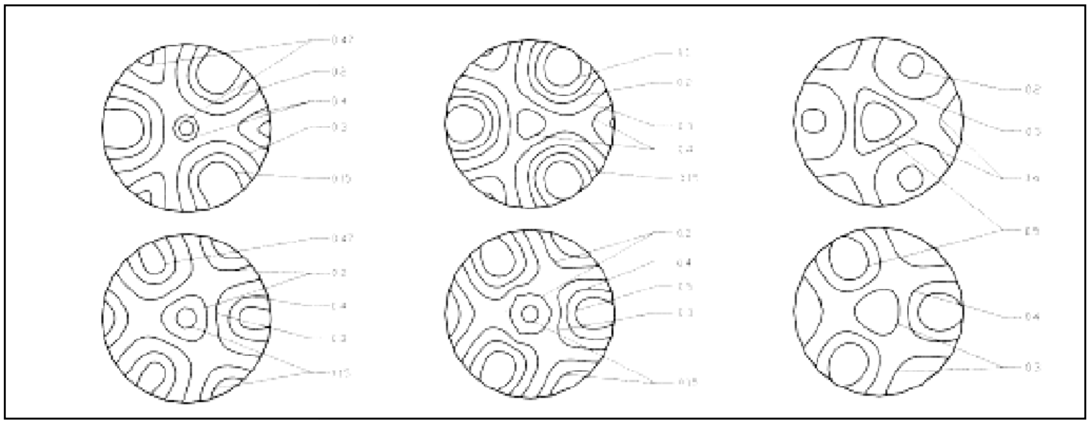

Figure 2.3. Stiffness maps of 3-DOF different spatial parallel manipulators [7]

The Jacobian and stiffness matrices are represented in an analytical form. The atlases of GCI (global conditioning index) and global stiffness index (GSI) are obtained in the solution space, which are used to optimize the link lengths of 3-DOF SPMs. The local dexterity and stiffness maps plotted in the reachable workspace can be used to study the dexterity and stiffness of the 3-DOF SPM. The results show that the atlases (or maps) of GCI (or local dexterity) are identical to those of GSI (or local stiffness), Figure 2.3. The problem of the computer-aided kinematic design of 3-DOF SPMs has been addressed in this article. It is indicated that the concepts of dexterity and stiffness are intimately related. Then, the tools are provided for the designer for optimizing the link lengths of manipulators and analyzing the dexterity and stiffness of 3-DOF SPMs on the reachable workspace. Examples of optimized 3-DOF SPMs and dexterity and stiffness maps are given and interpreted. Since the dexterity and stiffness are important issues in the context of parallel, the method can also be extended to other parallel manipulators.

The ability of a robot to react to external forces is defined as compliance. This characteristic is very important for a robot intended to perform assembly tasks. In this manner, a new architecture of a parallel robot with six degrees of freedom is presented in [8], Figure 2.4. In that study, the detailed characteristics and the geometric and kinematic models of the robot are discussed.

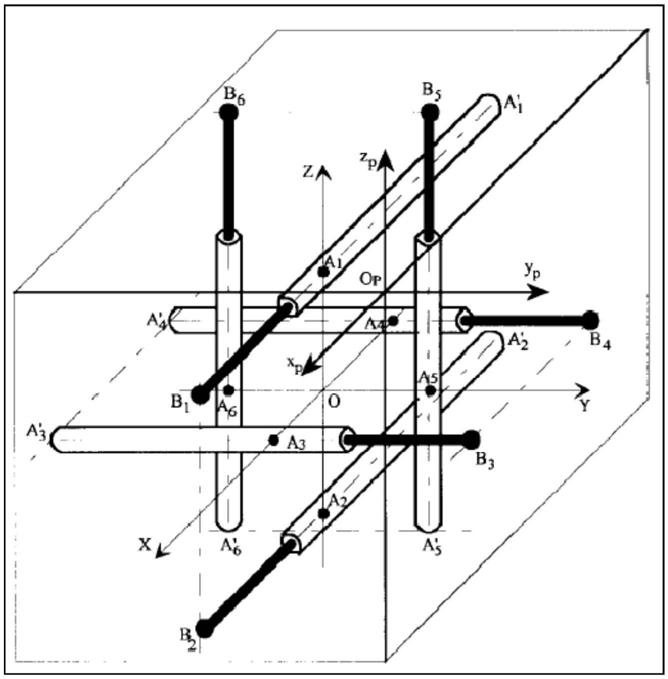

Figure 2.4. Spatial arrangement of the segments of C5 joint parallel robot [8]

The methods are analytically expressed and it is claimed that a direct geometric model was found in an analytical form by inverting the inverse kinematic solution. The comparison of computation times for each model is made and the inverse geometric model is found as the fastest, see Table 2.1. According to these solutions, a compliance study is conducted and the relations between the geometry and the compliance of the manipulator are represented.

Table 2.1. Evaluation of computation times for each model [8]

Models	**Computation Time(ms)**
Inverse geometric model	0.347
Direct geometric model	0.548
Inverse kinematic model	0.560
Direct kinematic model	1.420

After that, workspace of the robot is defined by both of the geometrical identifications and numerical inverse kinematic solution. According to results, the advantages of the manipulator over an equivalent size Stewart platform is reported as: larger ability to perform linear displacements along the three axes for an identical stroke of actuators, limited ability to perform angular displacements, higher rigidity due to the fact that the spherical joints are farther from each other than those of an equivalent sized Stewart platform.

Finally, the hardware and software control system are also described. It is claimed that this manipulator is well adapted to perform force feedback control. This robot has been designed in order to obtain a symmetric and compact structure. Due to the fact that each actuator keeps a constant orientation with respect to the static part, they show that the direct model has a single analytical solution. This result leads them to characterize the robot singularities and the reachable workspace. To demonstrate the capability of the proposed structure, an application of the C5 parallel robot acting as a force controlled active wrist in an assembly task is described.

2.2. STIFFNESS CRITERION

Another approach to get the optimal workspace and stiffness index according to given task is using modular parallel robots. These types of robots are mechanisms which can adapt their geometry according to the task to be performed, usually by changing the location of the attachment points of the legs on the base. The main ideas underlying this concept are that by changing the geometry of the robot one can extend the reachable workspace.

Merlet presents a study to improve the performances of the robot [9]. In this paper an algorithm is proposed which first adapts the geometry so that a set of given trajectories is included in the workspace of the robot and then optimize an arbitrary performance consideration with stiffness criterion.

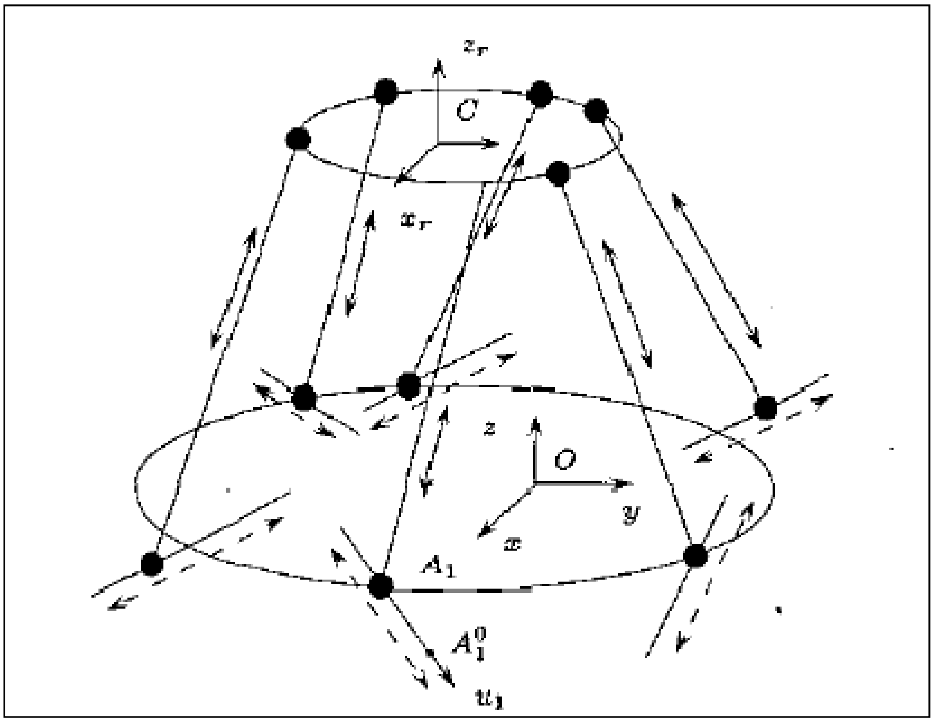

Figure 2.5. A classical Gough platform with modular manipulator representation [9]

It is shown that indeed modular parallel robot allow for drastic increase in the performance. In that case, a method to determine an optimal geometry that provides a large increase in the performance of the robot is presented, Figure 2.5.

Kim and Tsai [10] reported a study on design optimization of a parallel manipulator in order to minimize deflection at the joints. This paper introduces a 3-DOF translational parallel manipulator called Cartesian Parallel Manipulator (CPM). The manipulator consists of a moving platform that is connected to a fixed base by three limbs. Each limb is made up of one prismatic and three revolute joints and all joint axes are parallel to one another. In this way, each limb provides two rotational constraints to the moving platform and the combined effects of the three limbs lead to an over-constrained mechanism with three translational degrees of freedom. The manipulator behaves like a conventional XYZ Cartesian machine due to the orthogonal arrangement of the three limbs.

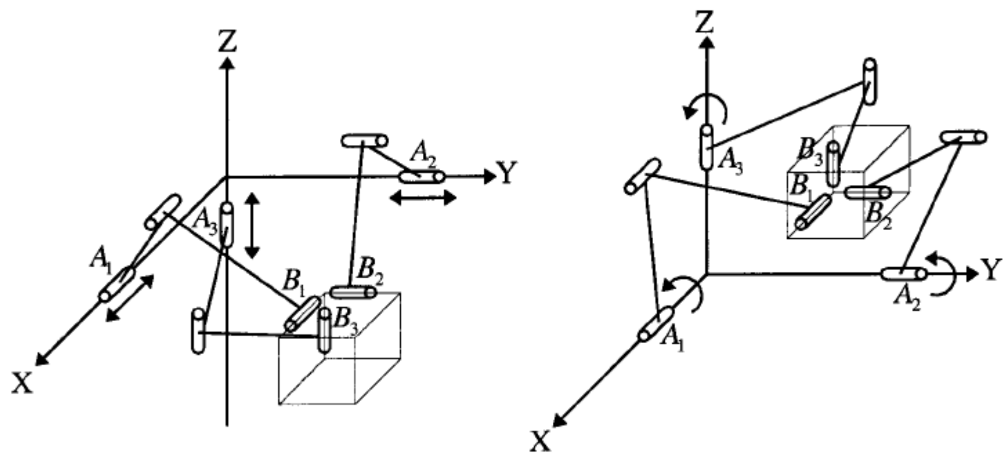

(a) Linear actuation method (b) Rotary actuation method

Figure 2.6. Linear and rotary actuation methods [10]

Two actuation methods are analyzed, in Figure 2.6. The analyses include the forward and inverse kinematics, the Jacobian analysis, the static force analysis, and the singularity analysis. However, the rotary actuation method is discarded because of the existence of singularities within the workspace. For the linear actuation method, there exists a one-to-one correspondence between the input and output displacements of the manipulator. The effects of misalignment of linear actuators on the motion of the moving platform are discussed. Each limb structure is exposed to a bending moment induced by external forces exerted on the moving platform. In order to minimize the deflection at the joints caused by the bending moment, a method to maximize the stiffness is suggested. The stiffness and workspace optimization of the manipulator is performed for the linear actuation method. Finally, a numerical example of the optimal design is presented and a prototype CPM has been constructed.

2.3. WORKSPACE OPTIMIZATION

A novel design for a 6-DOF parallel manipulator is presented in [11]. The design is a modification of the Stewart Platform that places the legs of the manipulator on two concentric circles both at the base and at the end effector. The legs can therefore cross over one another in space without interference, which allows them to move closer to the horizontal, Figure 2.7.

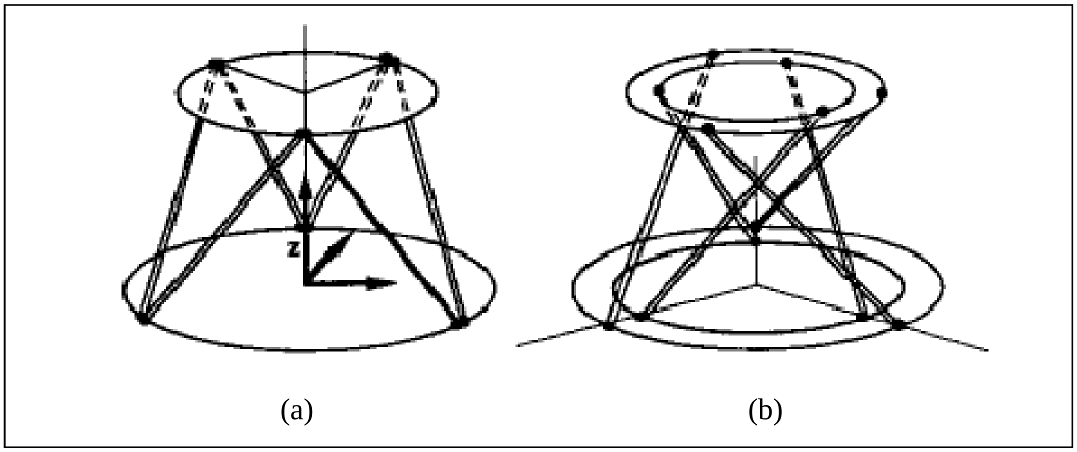

Figure 2.7. (a) The Stewart platform (b) the optimized manipulator [11]

This brings the force/torque and velocity capacities in different directions more into balance. Forward kinematic solution is shown and Jacobian matrix is analytically obtained from the derivative of forward kinematic equations.

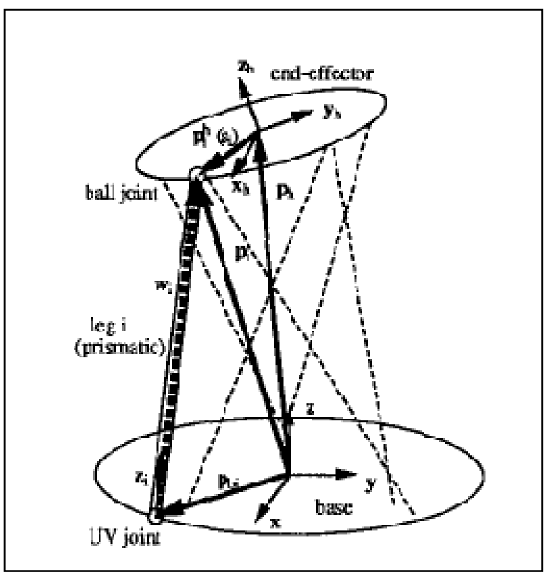

Figure 2.8. Geometry of one leg of the MSP manipulator [11]

The optimization consideration in this study is on the basis of the singular values of Jacobian. The degree of improvement attainable is quantified by defining a measure of dexterity as the average condition number of the Jacobian matrix. The condition numbers of various configurations are compared to find out the optimal design of the manipulator.

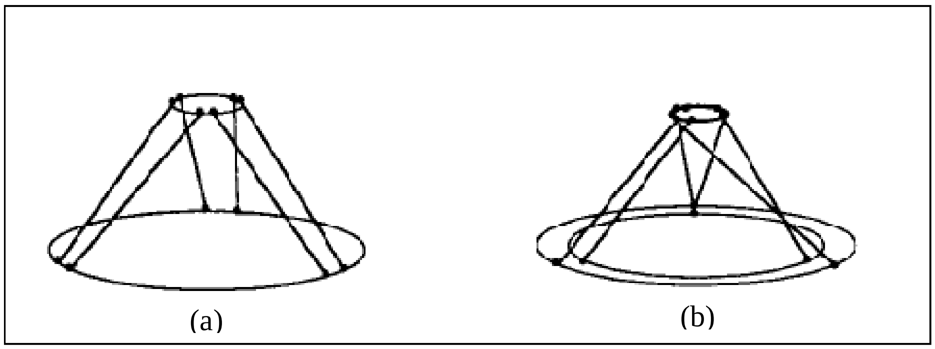

Figure 2.9. Representative optimized designs emphasizing dexterity,
(a) Stewart Platform, (b) MSP [11]

Several designs are analyzed and discussed under the consideration of workspace volume, where the workspace volume is presented in dimensionless form as the ratio $V/\Delta l^3$, and one of these designs is found to give optimal result. In conclusion, it is shown that the new design offers significantly improved dexterity (30%) over the traditional Stewart Platform design.

A new algorithm to optimize the length of the legs of a spatial parallel manipulator for the purpose of obtaining a desired dexterous workspace rather than the whole reachable workspace is introduced in [12]. A Schöenflies-type parallel manipulator with a desired dexterous workspace, Figure 2.10, is studied and a new methodology to optimize the lengths of the kinematic chains is reported. With the analysis of the degree of freedom of a manipulator, the method can be used to select the least number of variables to describe the kinematic constraints of each leg of a manipulator. In this way, kinematic analysis of the manipulator has been done and the desired workspace is used as an objective function to transform the problem to be an optimization problem. The optimum parameters are obtained by searching the extreme values of the objective functions with the given dexterous workspace. In addition, an example is utilized to demonstrate the significant advantages of this method in the dexterous workspace synthesis. In applications, it is claimed that, this method can be widely used to synthesize, optimize, and create all kinds of new spatial parallel manipulators with a desired dexterous workspace.

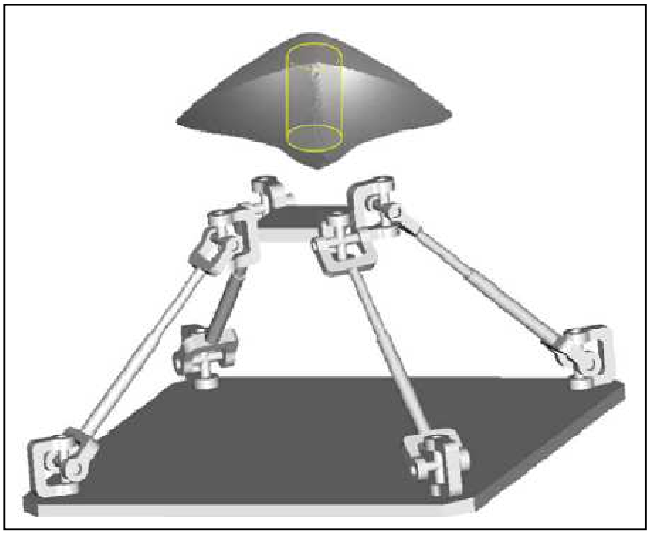

Figure 2.10. The required dexterous workspace and the mechanism [12]

Observing that regular (e.g., hyper-rectangular) workspaces are desirable for most machines, the concept of effective regular workspace, which reflects simultaneous requirements on the workspace shape and quality, are proposed. The effectiveness of such a workspace is characterized by the dexterity of the mechanism over every point in the workspace, [13]. In this research, it is claimed that the other performance indices, such as manipulability and stiffness, provide alternatives of dexterity characterization of workspace effectiveness. An optimal design problem, including constraints on active/passive joint limits and link interference, is then formulated to find the manipulator geometry that maximizes the effective regular workspace. This problem is defined as a constrained nonlinear optimization problem without explicit analytical expression Figure 2.11.

In this study, the controlled random search technique, which is reported as robust and reliable, is used to obtain a numerical solution. It is noted that the algorithm converges extremely fast initially. It takes only 253 function evaluations, which is less than 15% of the total effort, to approach the objective of 0.12872, which is about 99.3% of the optimum. The design procedure is demonstrated through examples of a Delta robot and a Gough-Stewart platform. An optimal design of Stewart platform is carried out to find dimensional parameters and a result is claimed to be the optimum for the objective of a prescribed workspace.

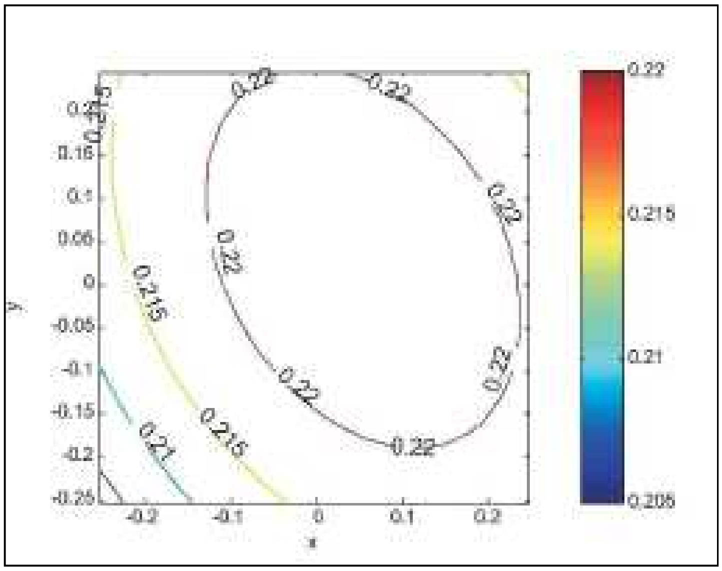

Figure 2.11. Counter plots of effective orientation workspace [13]

In another study, [14], the relationship between link lengths and workspace shape is studied. The relationship between the shapes of workspaces and the dimensions of manipulators is a good indicator to obtain the effective workspace. The relationship is first analyzed with classification of 3-DOF planar parallel manipulators. The several shapes of the workspaces for classified robots are presented; the relationships between the shapes of the workspaces and the link lengths of each of the classifications are presented. According to these analyses, some relations between the link lengths and workspace shapes are observed. The results of this paper are useful for the designers not only to understand the distribution of characteristics of the workspaces for various link lengths of 3-DOF PPMs, but also to optimize the manipulators.

Another requirement that represents the quality of the workspace is increasing the singularity free zones in the workspace. Arakelian and coworkers studied the increase in singularity free zones [15]. In this study, a pressure angle is defined as an indicator of the quality of motion transmission, and in their opinion such a kinetostatic approach shows the nature of the inaccessibility of parallel manipulators' singular zones better than the kinematic approach. The procedure is based on the known kinematic singularity equations and the control of the pressure angles in the joints of the manipulator along the given trajectory of the platform Figure 2.12. The zones, which cannot be reached by the manipulator, were detected. For increase of the reachable workspace of the manipulator a variable leg structure is proposed. Such a solution allows obtaining the best structural architecture of the manipulator for any trajectory.

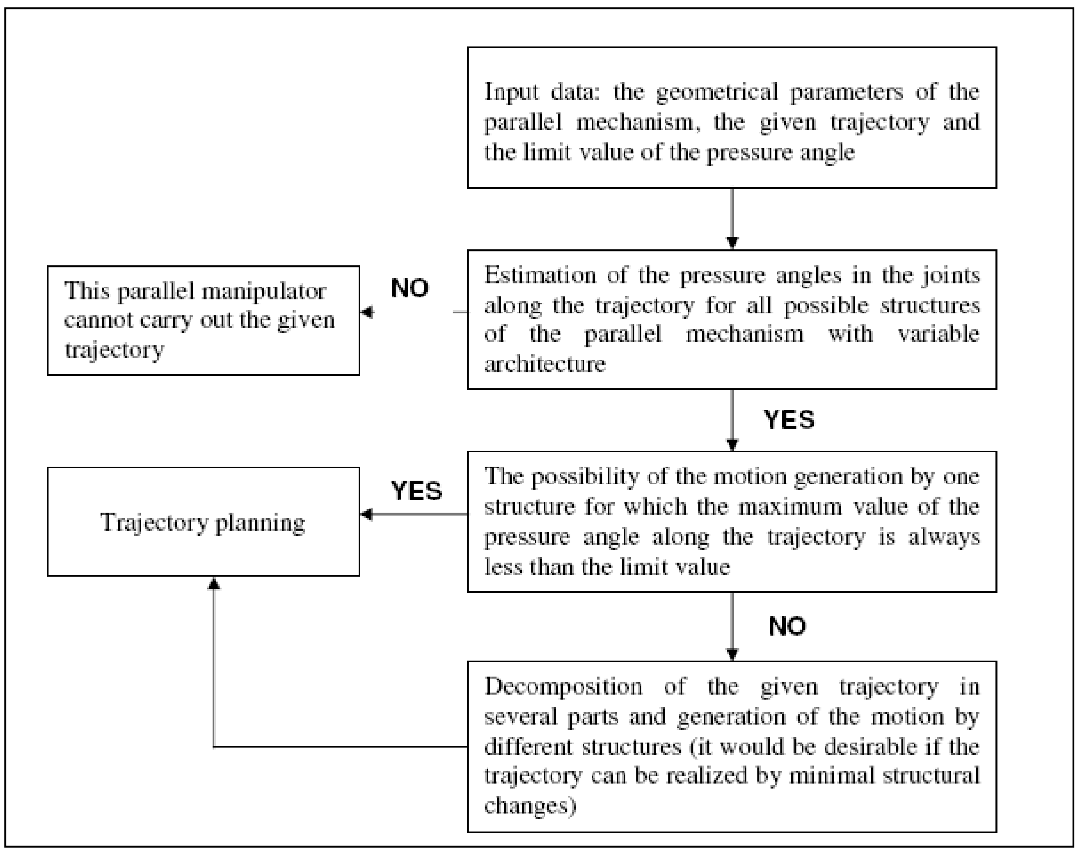

Figure 2.12. Procedure for determination of the optimal structure of the parallel manipulator taking into account the limit pressure angle [15]

The design of the optimal structure of the planar parallel manipulator 3-RPR was illustrated by two numerical simulations. It is believed that the suggested method is a useful tool for the improvement of the functional performance of parallel manipulators with singular zones Figure 2.13.

Table 3
Total value of singularity-free volumes for each case of actuation

Type of actuation	$\phi = 0°$ (workspace surface: 0.21 m^2)		$\phi = 45°$ (workspace surface: 0.2 m^2)	
	Singularity-free zones (m^2)	Singularity-free zones relative to the whole workspace (%)	Singularity-free zones (m^2)	Singularity-free zones relative to the whole workspace (%)
RRR	0.137	65	0.147	74
PPP	0.181	86	0.152	76
PRR	0.152	72	0.158	79
RPR	0.152	72	0.158	79
RRP	0.152	72	0.158	79
RPP	0.155	74	0.165	83
PRP	0.155	74	0.165	83
PPR	0.155	74	0.165	83

Figure 2.13. The result table of different robot structures considering the total singularity free volume of the translational workspace [15]

The optimization of the workspace with an operation performance of the manipulator is another search area. In another research [16], the optimum design issue of a 5R symmetrical parallel manipulator with a surrounded workspace is concerned, Figure 2.14. Generally, such a manipulator has a very large workspace. With different working modes, a manipulator will have different internal singularities and workspaces. In this paper, the singularity and the usable workspace without singularities is tried to be determined for the manipulator with specified geometry.

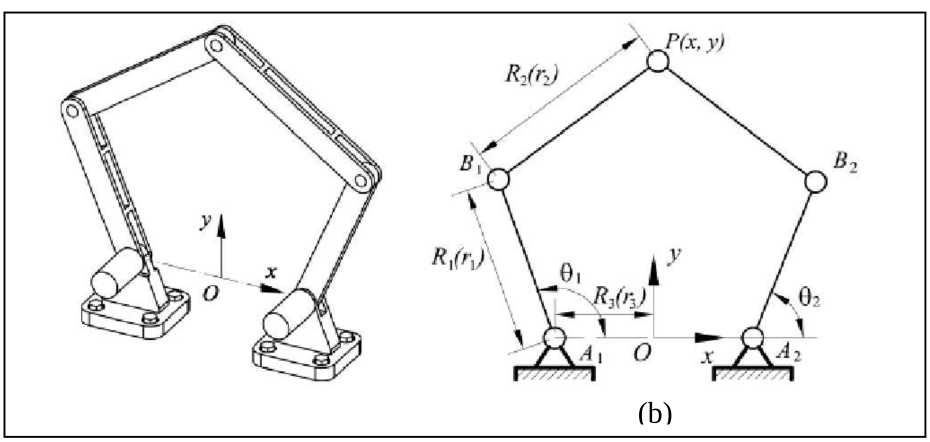

Figure 2.14. The 5R parallel manipulator [16].

The usable workspace can be used to define the global conditioning index (GCI). In order to obtain the optimum design of the manipulator, a non-dimensional design space is also established in this study. Because each of the non-dimensional manipulators in the established design space can represent the performances of all of its possible similarity manipulators, the design space is a very useful tool for guaranteeing a global comparative result.

Within the design space, the singularity, usable workspace, and control accuracy (evaluated using the GCI) are studied and the corresponding atlases are constructed. Based on the atlases, one can synthesize link lengths of the manipulator studied with respect to specified criteria. One is given to show how to use the atlases. In particular, an example is presented of reaching the optimum dimensional result with respect to a desired practical workspace based on the optimum non-dimensional result identified from the atlases. For the reason that using the atlases presented in this paper a designer can obtain the optimum result with respect to any specification, the optimum design method proposed in this paper may be accepted by others.

Majid, Huang [17] and Yao studied on the workspace of a six-degrees-of-freedom parallel manipulator of the general three-PPSR type manipulator. This type actually has the same topology as the Yeditepe Parallel Manipulator.

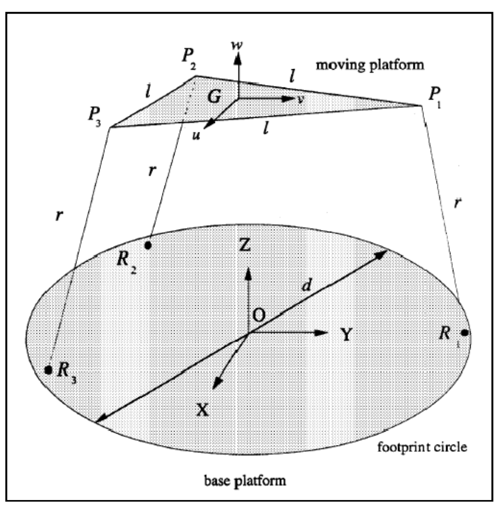

Figure 2.15. A 3-PPSR parallel manipulator [17]

The mechanism of a three-PPSR manipulator and its variations are briefly analyzed in this study. The workspace is then investigated under the physical constraints of slider and spherical joint limitations, and the effects of joint limit and link interference on the workspace shape and size are numerically studied. The constituent regions of the workspace corresponding to different classes of manipulator poses are discussed. It is shown that the workspace of this parallel manipulator is larger than that of a comparable Stewart platform, especially in the vertical direction, Figure 2.16.

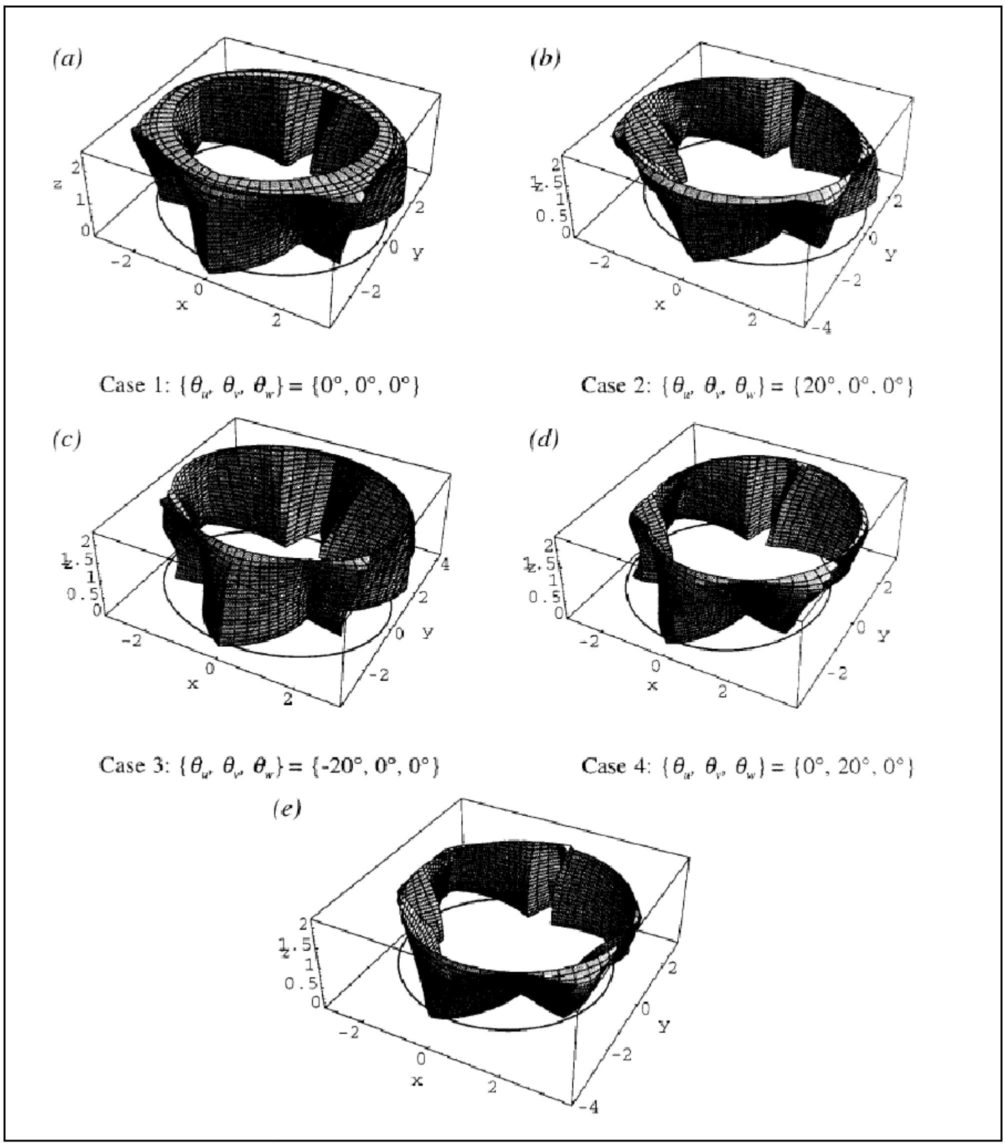

Figure 2.16. Theoretical workspace boundaries of a three-PPSR manipulator [17]

This study proves that there is a big need in the optimization of the orientation workspace. Although some researcher has focused on the modeling and the analysis of the orientation workspace, there is almost no study about the optimization of the orientation workspace when a high rotation capability manipulator is concerned.

3. TOPOLOGY OF THE YPM MANIPULATOR

The term topology was first introduced into robotics to characterize the kinematic structure of a manipulator without reference to its dimensions. In order to address fundamental issues in kinematic synthesis, one has to introduce essentials into the concept of topology through the analysis of representative architectures, to propose a topological representation which provides a better correspondence between the representation and the intended manipulators.

To facilitate the kinematic analysis, kinematic synthesis, classification, and comparison studies of manipulators, the terms kinematic composition, topology, and their definitions are proposed as follows [18]:

- the kinematic composition of a manipulator is the essential information about the number of its links: which link is connected to which other links, by what types of joints, and which joints are actuated,
- the topology of a manipulator is its kinematic composition plus the essential constraints.

3.1. PRELIMINARIES

A review of some basic concepts and definitions about kinematic chains are necessary as a starting point of discussion on topology and topological representation.

- A kinematic chain is a set of rigid bodies, also called links, coupled by kinematic pairs.
- A kinematic pair is, then, the coupling of two rigid bodies so as to constrain their relative motion. Kinematic pairs are classified as upper pairs and lower pairs.
- An upper kinematic pair constrains two rigid bodies such that they keep a line or point contact.
- A lower kinematic pair constrains two rigid bodies such that a surface contact is maintained.

A joint is a particular mechanical implementation of a kinematic pair. As shown in Figure 3.1, there are six types of joints corresponding to the lower kinematic pairs – spherical (S), cylindrical (C), planar (E), helical (H), revolute (R), and prismatic (P). Since all these joints can be obtained by combining the revolute and prismatic ones, it is possible to deal only with revolute and prismatic joints in kinematic modeling.

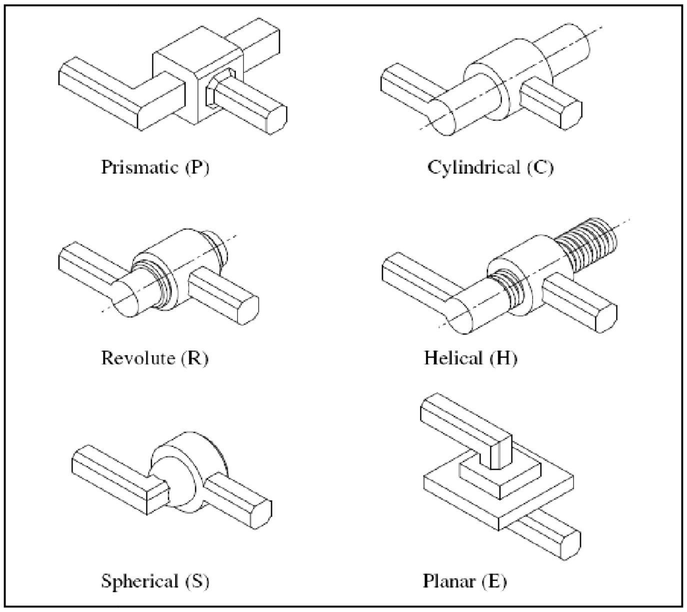

Figure 3.1. Lower kinematic pairs [18]

Moreover, all these joints can be represented by elementary geometric elements (i.e., points and lines). To characterize links, the notions of simple link, binary link, ternary link, quaternary link, and n-link were introduced to indicate how many other links is connected to a link. Similarly, binary joint, ternary joint and n-joint indicate how many links are connected to a joint. A similar notion is the connectivity of a link or a joint. These basic concepts constitute a basis for kinematic analysis and kinematic synthesis.

3.2. TOPOLOGICAL REPRESENTATION

The basic notions about link and joint introduced in Section 3.1. are used to describe manipulator kinematics. With these notions, the general spatial arrangement of links and joints of a manipulator can be described with ease. One of the more visual representation methods is the kinematic diagram. A kinematic diagram is a drawing of a mechanism showing its essential elements in simplified form with graphical symbols shown in Figure 3.2.

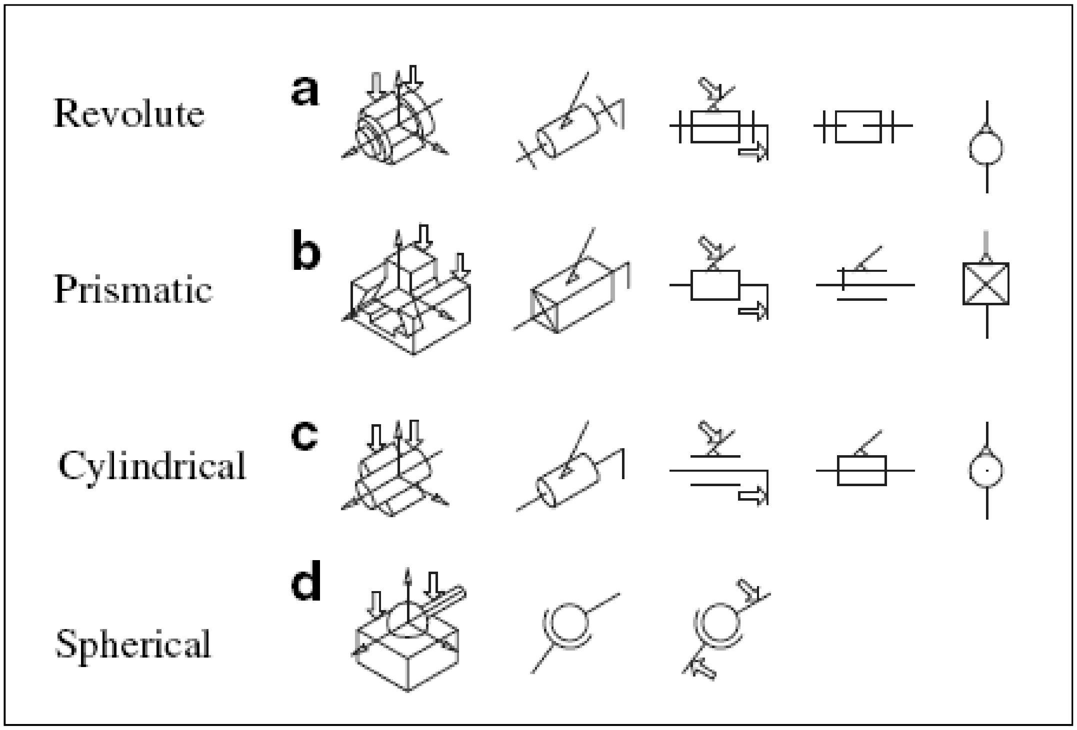

Figure 3.2. Kinematic joint symbols [18]

3.3. KINEMATIC COMPOSITION OF THE YPM

Yeditepe Parallel Manipulator is composed of three identical legs, three revolute joints, six linear actuators, one mobile platform, and one base platform, Figure 3.3. The simplifications for topological representation are made as follows:

- legs are simplified to links,
- revolute joints are modeled as R joints,
- actuators are simplified to prismatic joints (P),
- platforms are simplified to circles.

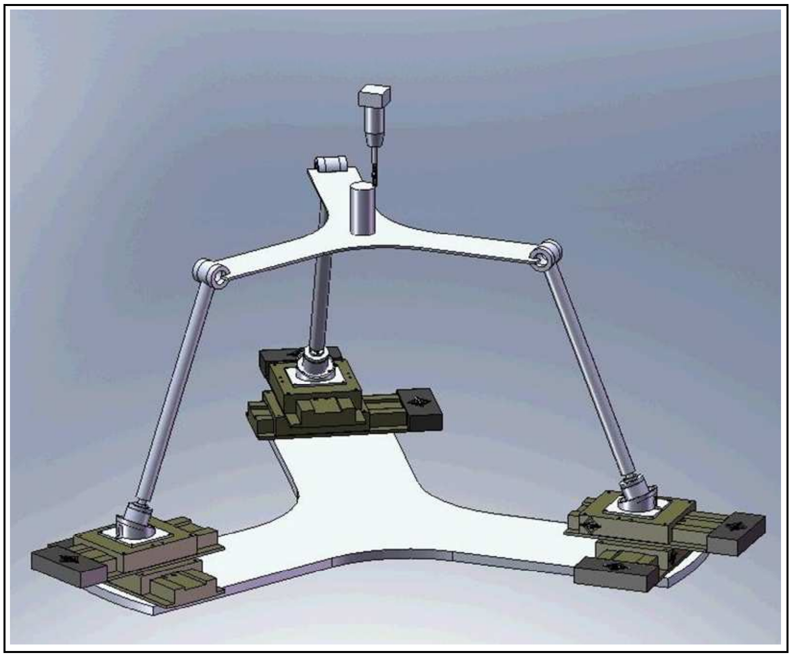

Figure 3.3. A simple illustration of the YPM

A sensitive plane motion is obtained by locating one actuator perpendicularly on another, shown in Figure 3.4. Therefore, three XY-tables are created by using six actuators. These tables are symmetrically mounted on a circle with a $120°$ separation on the base plane. The radius of the base circle is symbolized with R_B, as shown in figure Figure 3.5. In this joint configuration, the prismatic ones are active, where the others are all passive joints.

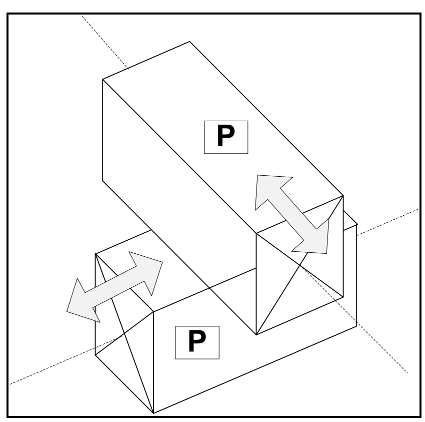

Figure 3.4. Assembly of X-Y tables

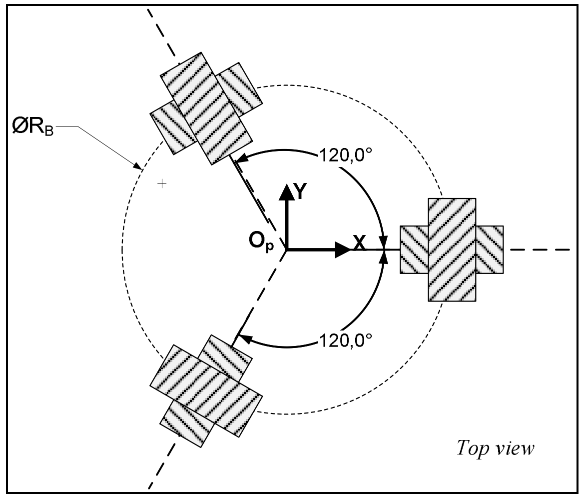

Figure 3.5. Assembly of XY-tables on the base platform

Three legs are connected to the tables using spherical joints. The upper ends of the legs are attached to the platform symmetrically with a 120° separation, the same on the base circle by revolute joints, illustrated in Figure 3.6. Here the radius of the platform circle is symbolized with ρ. In summary, the Yeditepe Manipulator is composed of three XY-tables mounted on the base plane, three spherical joints that connect the legs to the tables and three revolute joints that attach the legs to the platform.

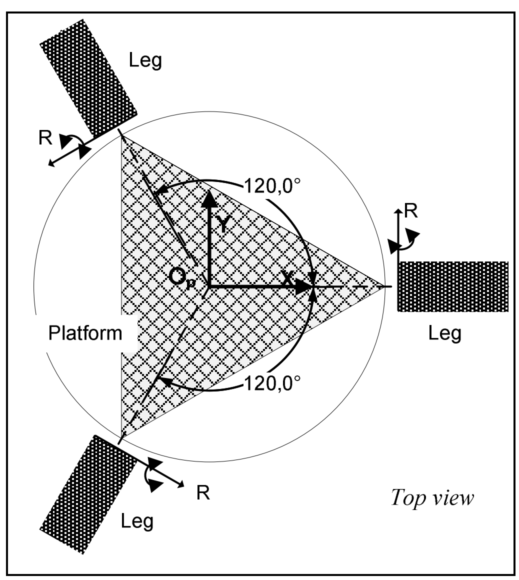

Figure 3.6. Assembly of the legs to the platform

It is of great importance that high precision manipulators are well designed from a mechanical point of view. A detailed analysis of an accurate manipulator indicates that the actuator precision plays a big role when positioning accuracy of the manipulator is concerned. There are only a few options exist in the market for high precision stages. One of them is Aerotech® ABL1000 air bearing stage with following specifications.

Table 3.1. ABL1000 specification sheet [19]

Resolution	0.5 nm
Maximum Travel Speed	300 mm/s
Maximum Linear Acceleration	10 m/s^2
Maximum Load	15.0 kg
Accuracy	±0.2 μm
Repeatability	±50 nm
Flatness	±50 nm
Range	±50 mm

Aerotech® ABL1000 air bearing stages were determined to use in this project because of their excellent accuracy and resolution features.

Figure 3.7. ABL1000 air bearing stages [19]

3.4. TOPOLOGY OF THE YPM

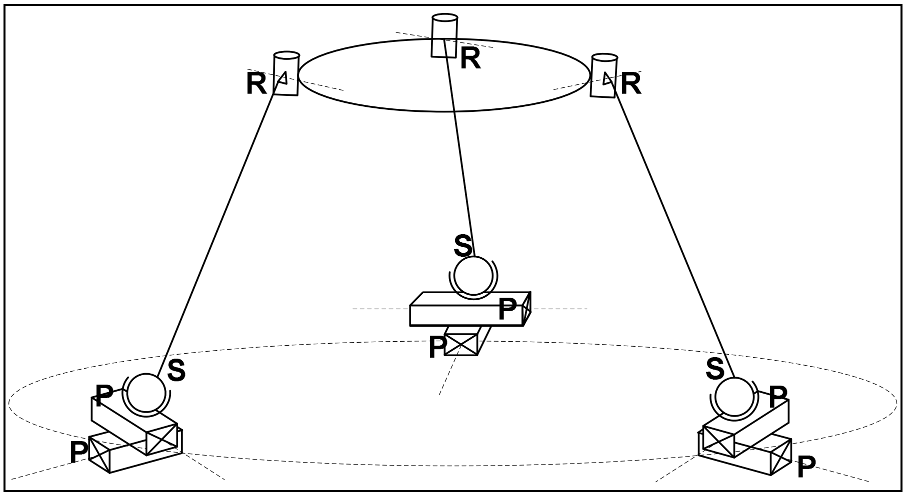

Figure 3.8. Kinematic diagram of theYPM

The air bearing stages and the spherical joints have physical limitations such as the translational and rotational ranges, maximum load capacity, maximum speed, maximum acceleration, and so on. In this study only the translational limitation of the stages is considered as the essential constraint.

After the definition of the kinematic composition and essential constraints of the YPM, a simplified kinematic diagram can be established, as shown in Figure 3.8.

3.5. MOBILITY OF THE YPM

The mobility of a mechanism is its number of degrees of freedom. Number of degrees of freedom of a mechanism can be generalized in the following formula, which is called Gruebler's Equation:

$$m = 6(n-1) - 5j_1 - 4j_2 - 3j_3 - 2j_4 - j_5 \tag{3.1}$$

where m is total degrees of freedom in the mechanism, n is number of links, j_1 is number of joints with one DOF, j_2 is number of joints with two DOF, and j_3 represents the number of joints with three DOF and so on. In this case, n is 8 (2 platforms, 3 legs, 3 XY-tables), $f_1=0$, $f_2=0$, $f_3=3$ (3 spherical joints), $f_4=3$ (3 x-y tables) and, $f_5=3$ (3 revolute joints). Therefore, the mobility of YPM is determined as six.

4. KINEMATICS OF THE YPM

Kinematics is the science of motion that treats motion without regard to the forces that causes it. Within the science of kinematics one studies the position, velocity, acceleration, and all higher order derivatives of the position variables.

Kinematics can be classified in two parts: forward kinematics and backward kinematics. In forward kinematics, manipulator's prescribed reference point position and orientation are computed by using the position of actuators. Inverse kinematics is the way of the calculation of the actuator positions by using the reference point position and orientation. In this study, inverse kinematics is often used to calculate the sliders positions to check the existence of a solution to platform's position and orientation at that instant.

4.1. INVERSE KINEMATICS OF THE YPM

The inverse kinematic analyses are generally solved by using the vectorial loops. In the Yeditepe Micromachining Manipulator, there are two coordinate systems: the base coordinate system (located at the origin of the base circle O_B whose axes are symbolized with capital letters) and the platform coordinate system (located at the centroid of the platform O_P).

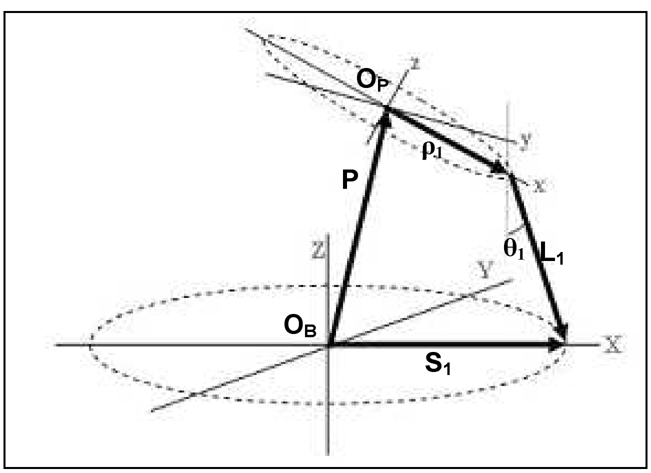

Figure 4.1. One of the vectorial loops of the YPM

In the Figure 4.1, the vectorial chain of the manipulator is illustrated. The vectorial chain is created through the base coordinate system, platform coordinate system and one of the legs. The other two chains can also be created by using the other two legs. In this figure $\vec{P}$ is the vector of the position of the platform according to the base coordinate system, $\vec{\rho}_1$ is the vector between O_P to the leg connection point of the platform, and $\vec{L}_1$ is vector of the leg connection point of the platform to the XY-table that lies on the base plane, $\vec{S}_1$ defines the position of the stage relative to the base frame. In this scheme, the leg connection point of the platform is a revolute joint and it is modeled as a plane vector. An angle θ_1 can be defined to set the rotation of the leg vector, where it is on the xz plane of the platform frame.

The trick in the solution is to define the vectors of $\vec{\rho}_1$and $\vec{L}_1$ with respect to the platform coordinate system, where these vectors are stationary on platform frame. Then, the position of the XY-table can be expressed in the platform frame.

Let’s say the radius of the platform is ρ and the length of the leg is L, therefore X-Y table position relative to platform is;

$$\begin{bmatrix} \rho \\ 0 \\ 0 \end{bmatrix} + L \begin{bmatrix} sin\,\theta_1 \\ 0 \\ -\,cos\,\theta_1 \end{bmatrix} = \ {}^{P}\vec{S}_1 \tag{4.1}$$

The other two legs are symmetrically connected to the platform with $120°$ separation, as mentioned in Section 3.3. The other vectorial chains can be created by multiplication of Equation 4.1 with a specific rotation matrix. The rotation matrices represent the rotation about platform z axis with the rotation amount, 0, $2\pi/3$ and $4\pi/3$ radians, respectively. Therefore the vectorial chains can be represented as;

$$\tilde{R}_i \left(\begin{bmatrix} \rho \\ 0 \\ 0 \end{bmatrix} + L \begin{bmatrix} \sin\theta_i \\ 0 \\ -\cos\theta_i \end{bmatrix} \right) = \ {}^{P}\vec{S}_i \tag{4.2}$$

where i$=1, 2, 3$.

$\tilde{R}_i$ can be expressed as;

$$\tilde{R}_i = \begin{bmatrix} \cos\left(\frac{2\pi}{3}(i-1)\right) & -\sin\left(\frac{2\pi}{3}(i-1)\right) & 0 \\ \sin\left(\frac{2\pi}{3}(i-1)\right) & \cos\left(\frac{2\pi}{3}(i-1)\right) & 0 \\ 0 & 0 & 1 \end{bmatrix} \tag{4.3}$$

The next step is to define vectorial chains relative to base coordinate system. The new relations come up with the rotation matrix that describes the orientation of the platform relative to base frame, $\tilde{R}_P$ and platform position vector $\vec{P}$. Therefore the vectorial chains with respect to base coordinate system are

$$\tilde{R}_P \tilde{R}_i \left(\begin{bmatrix} \rho \\ 0 \\ 0 \end{bmatrix} + L \begin{bmatrix} \sin\theta_i \\ 0 \\ -\cos\theta_i \end{bmatrix} \right) + \vec{P} = {}^{B}\vec{S}_i \tag{4.4}$$

It is known that the XY-tables are on base plane and their z components are zero.

$$\tilde{R}_P \tilde{R}_i \left(\begin{bmatrix} \rho \\ 0 \\ 0 \end{bmatrix} + L \begin{bmatrix} \sin\theta_i \\ 0 \\ -\cos\theta_i \end{bmatrix} \right) + \vec{P} = \begin{bmatrix} x_i \\ y_i \\ 0 \end{bmatrix} \tag{4.5}$$

where x_i and y_i are the position of the x-y tables relative to base coordinate frame. Now the third row equation is

$$\begin{bmatrix} \tilde{R}_P \tilde{R}_{i_{(31)}} & \tilde{R}_P \tilde{R}_{i_{(32)}} & \tilde{R}_P \tilde{R}_{i_{(33)}} \end{bmatrix} \begin{bmatrix} \rho + L\sin\theta_i \\ 0 \\ -L\cos\theta_i \end{bmatrix} + \vec{P}_Z = 0 \tag{4.6}$$

Therefore,

$$\tilde{R}_P \tilde{R}_{i_{(33)}} \cos\theta_i - \tilde{R}_P \tilde{R}_{i_{(31)}} \sin\theta_i = \frac{\tilde{R}_P \tilde{R}_{i_{(31)}} \rho + P_Z}{L} \tag{4.7}$$

All the variables except θ are known. Now the unknown θ_i can be solved as;

$$-Asin\beta sin\theta_i + Acos\beta cos\theta_i = \frac{\tilde{R}_P \tilde{R}_{i_{(31)}} \rho + \vec{P}_Z}{L} \tag{4.8}$$

$$\theta_i = -\beta \mp cos^{-1}(\frac{\tilde{R}_P \tilde{R}_{i_{(31)}} \rho + \vec{P}_Z}{AL}) \tag{4.9}$$

It is easily seen from Equation 3.9, θ has two solutions. When the other two legs are considered, the inverse kinematics gives $2^{number\ of\ \theta}$ solutions, which is eight.

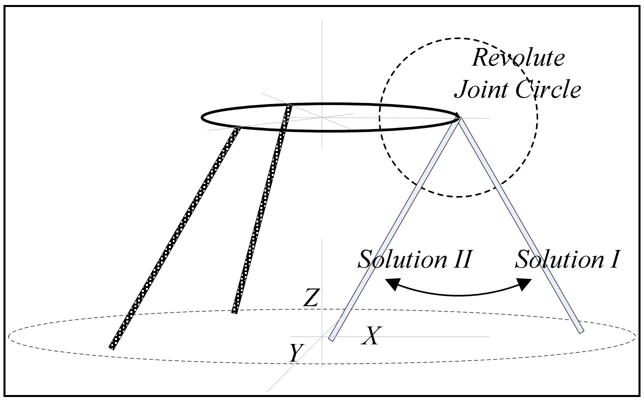

Figure 4.2. Multiple solutions of the inverse kinematics of the YPM

The fact that a manipulator has multiple solutions may cause problems because the system has to be able to choose one. The criteria upon which to base decision vary, but a very reasonable choice would be the closest solution. Therefore in the situation of the multiple solutions, the inverse kinematic solution should choose the closest solution to the one step back in the time history.

After the solution of the three θ, they are put back in to Equation 4.4 and the slider positions are calculated relative to the base frame. The next step is to transform slider positions in to the slider frame coordinates. A set of rotation matrices are defined to describe the slider frames.

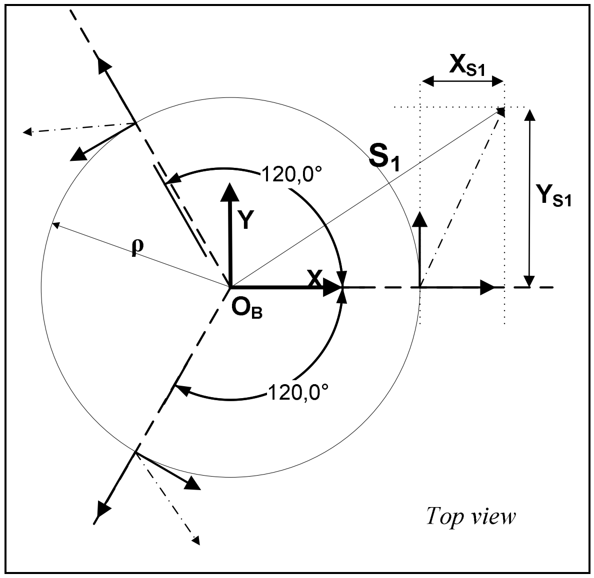

Figure 4.3. Slider positions relative to slider frames

In Figure 4.3, R_B is radius of the base circle, X_{Si} and Y_{Si} are slider positions with respect to the slider coordinate frames. The rotation matrix that transforms the vectors from slider frame to base frame is the same as the matrix represented in Equation 4.3.

$$\tilde{R}_{Si} = \begin{bmatrix} cos\,(\frac{2\pi}{3}(i-1)) & -sin\,(\frac{2\pi}{3}(i-1)) & 0 \\ sin\,(\frac{2\pi}{3}(i-1)) & cos\,(\frac{2\pi}{3}(i-1)) & 0 \\ 0 & 0 & 1 \end{bmatrix} \tag{4.10}$$

where i $= 1, 2, 3$ and, transformation equation is;

$$\tilde{R}_{Si} \begin{bmatrix} R_B + X_{Si} \\ Y_{Si} \\ 0 \end{bmatrix} = \begin{bmatrix} X_i \\ Y_i \\ 0 \end{bmatrix} \tag{4.11}$$

Inverse kinematic solution gives the slider positions relative to the slider frames if the position and the orientation of the platform are known. For a more specific solution, the limitations of the sliders can be added to the solution to restrict platform motion. A MATLAB algorithm is developed to calculate slider positions and it warns the user if there are no solutions, or slider limits are exceeded.

5. WORKSPACE ANALYSIS OF THE YPM

The workspace of a robot is one of its most important parameters reflecting its working capacity. The workspace of the YPM is defined as the set of all mobile platform poses (position and orientation) which can be reached by some choice of slider positions. As the reachable positions of mobile platform are dependent on its orientation a complete representation of the workspace should be embedded in a 6-dimensional space for which human-understandable representation may exist. Several types of three-dimensional representations are investigated. For instance, when the orientation is fixed, the 6-DOF workspace reduces to a 3-DOF workspace, usually referred as the ‘‘positional workspace’’ or the ‘‘constant orientation workspace’’. Alternatively, when the position is fixed, the 6-DOF workspace reduces to a 3-DOF workspace, usually referred as the ‘‘orientation workspace’’. In this manner, the constant orientation workspace is the set of locations of the moving platform that may be reached when the orientation is fixed, and the orientation workspace is the set of all doable orientations when the position of the position is fixed.

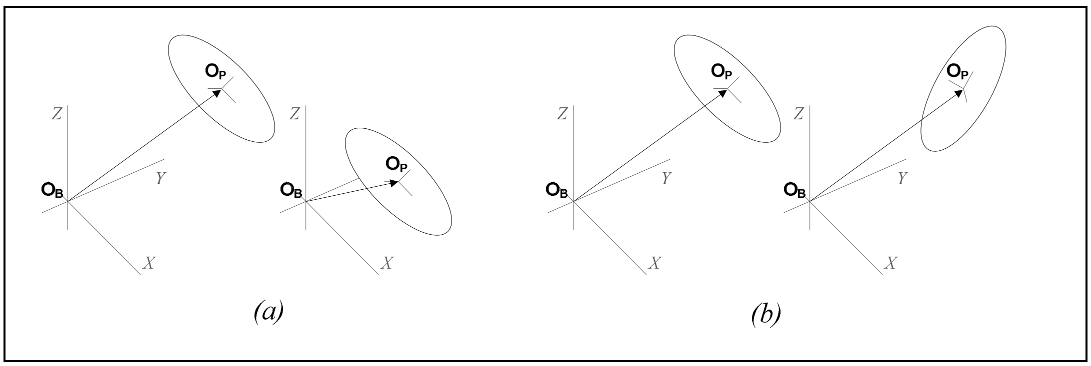

Figure 5.1. a) Two different positions of the moving platform with same orientation, b) Two different orientations of the moving platform with same position

Among other performance of the parallel manipulators mentioned in Section 2.1, and Section 2.2. The size and shape of the workspace are some of the major considerations in the design and analysis of the YPM. When the YPM is considered as a parallel machining unit with a fixed spindle, it is essential to analyze its machining workspace and boundary machining workspace in order to expand its range of applications. Additionally, it is essential to judge if a workpiece can be cut by the YPM Machining Unit according to its pose (position and orientation).

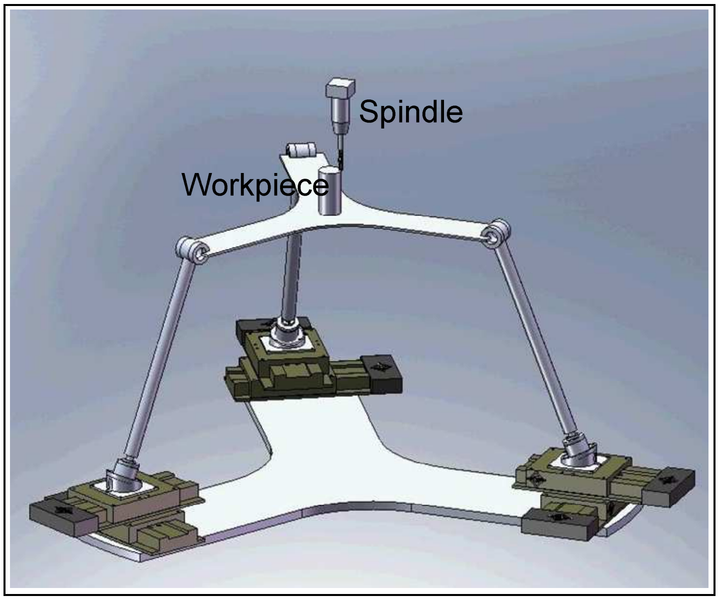

Figure 5.2. The YPM Machining Unit

The purpose of this study is to present the effect of geometric design on the YPM workspace and to optimize it. Unlike conventional milling, free form surface milling requires approaching to the workpiece with various orientations. It means that rotational capability of the moving platform plays an important role for machining.

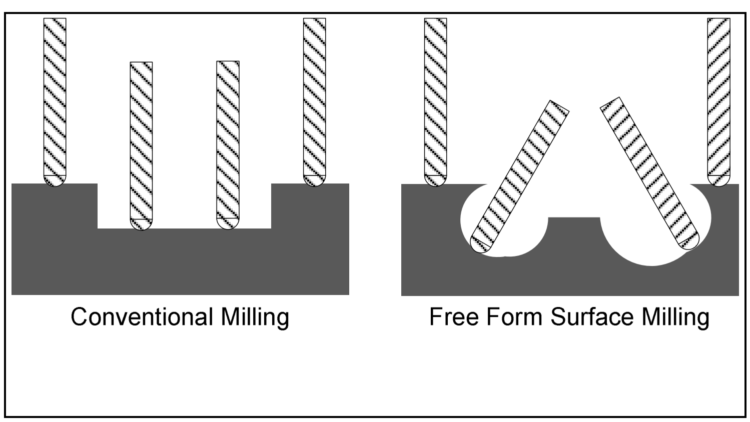

Figure 5.3. Illustration of machining types

Therefore, it is required to get the maximal orientation workspaces for every position of the platform. In such cases, a new definition should be made, named as "the *maximal workspace*." The maximal workspace can be defined as the set of positions that may be reached and the maximal orientation workspaces at those positions. Therefore the entire orientation space at every reachable position of the platform needs to be swept to find out the maximal orientation workspace for that position of the platform.

Another issue is the representation of workspace. The representation of the translational (position) workspace is relatively simple and straightforward. However, the representation of the orientation workspace is a more complex and challenging task.

The orientation workspace can be defined by numerous parameterization approaches such as the Roll–Pitch–Yaw angles, the direction cosine matrix (DCM), Euler axis and angle (rotation vector), Euler angles, tilt and torsion angles, quaternions, Rodrigues parameters as well as Cayley–Klein parameters. Even for Euler angles, there are twelve possible conventions.

5.1. TRANSLATIONAL WORKSPACE REPRESENTATION

The position of the moving platform is defined with a *3x1* vector in Cartesian space, as shown in Section 4.1. Every position vector corresponds to a point in the Cartesian space. The totality of all such points forms a point cloud, connected or not.

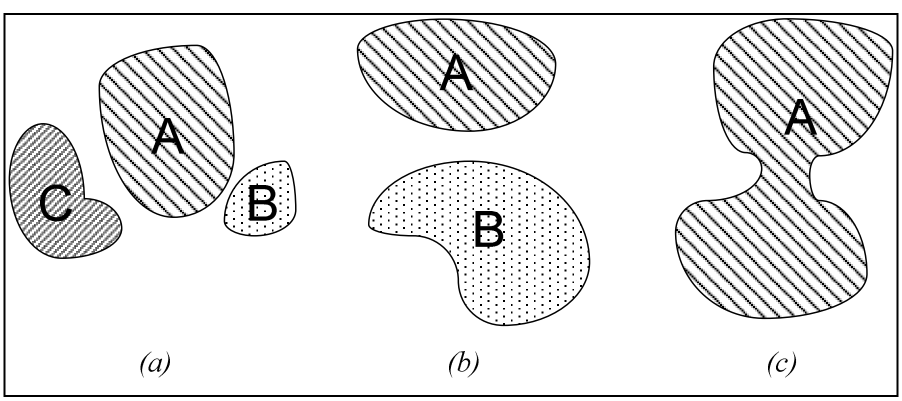

Figure 5.4. Demonstration of 2D translational workspaces

In Figure 5.4, three different translational workspaces are demonstrated which are composed of connected or not connected point cloud(s). In Figure 5.4 (a), there are three different regions that are not connected. Actually these regions represent the different solution sets of kinematic analysis. The different solution sets of a workspace are referred as kinematic circuits in mechanisms literature. The kinematic circuits can also be defined as the regions of possible motion sets in a workspace. The disconnected circuits are not reachable from one another.

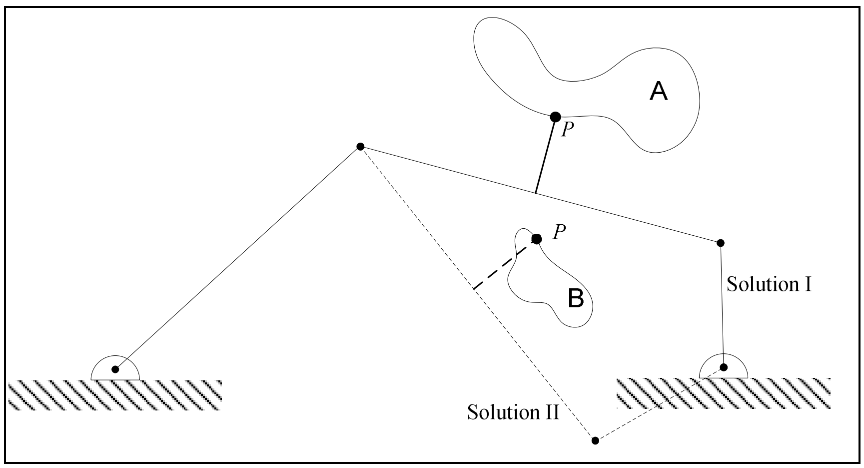

Figure 5.5. Kinematic circuits of a 4-bar mechanism

A 4-bar mechanism is given as an example to explain the kinematic circuits of mechanisms, in Figure 5.5. In the example, an identified point P on the mechanism can follow two different possible trajectories A and B. These trajectories are defined as the kinematic circuits of the mechanism and will be demonstrated with two different regions in the translational workspace. Since these two circuits do not intersect (not connected), the mechanism cannot pass from one trajectory to the other. However, when the mechanism is in the first circuit, by physically disconnecting one of the revolute joints, the link can be rotated and reassembled in to the second circuit. These different assembly configurations are named as assembly modes of the mechanism. Although the motion of the mechanism appears to be different, depending on the circuit of operation, the relative motion between the links does not change. The circuit in which the mechanism is assembled must be determined according to the operation of the mechanism. Therefore the maximal workspace in Figure 5.4 (b) is not the totality of the regions A and B. Because when the circuit A is selected, the circuit B is not applicable and vice versa. However in Figure 5.4 (c), the entire region is reachable. It means that all the points in the region A can be used for path planning of the mechanism. Therefore a workspace is not the totality of the regions. It consists of the region at which mechanism is in and the connected regions.

When the translational workspace boundaries of the YPM are considered, it is observed that maximum translations in x and y directions are not dependent on the dimensional configuration. This is because the sliders can move freely on xy plane together as shown in Figure 5.6. Therefore the workspace optimization is only considered in the z direction of the translational workspace.

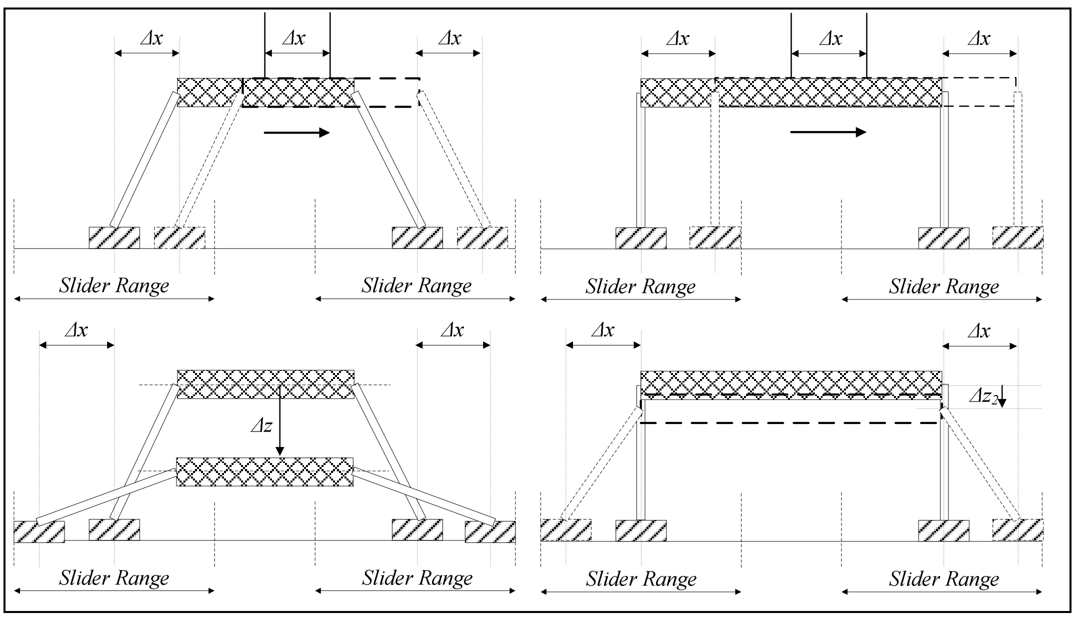

Figure 5.6. Illustration of the effect of the dimensional configuration on the translational workspace of the YPM

5.2. ORIENTATION WORKSPACE REPRESENTATION

The most widely-known method to describe the orientation of a rigid body is to attach a frame to it. After defining a reference coordinate system, the orientation of the rigid body is fully described by the orientation of its axes, relative to the reference frame.

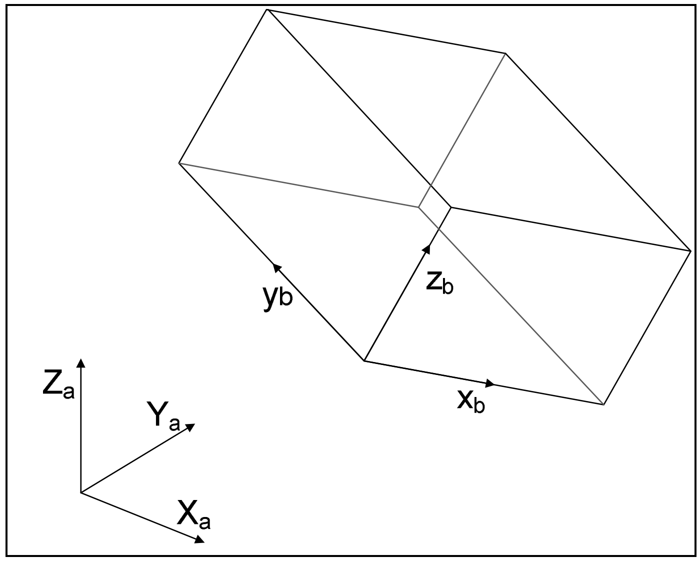

Figure 5.7. The description of the orientation of a rigid body by attaching a frame to it

A rotation matrix is often used to describe the relative orientation of two such frames. The columns of this 3 × 3 matrix consist of the unit vectors along the axes of one frame, relative to the other, reference frame. Thus, the relative orientation of a frame $\{b\}$ with respect to a reference frame $\{a\}$ is given. Although the rotation matrix has nine variables, three of them are independent. The rotation matrices in this study are used to describe the orientations of the frames located on the revolute joints relative to the platform and the orientation of the platform relative to the base frame, in Section 4.1.

All of the methods mentioned in Chapter 5, lead to the rotation matrix. They are applied to parameterize the rotation matrix. In this study, the orientations are parameterized in several methods as follows.

- Equivalent Angle-Axis Representation,
- Rodrigues Parameters,
- XYZ Fixed Angles.

The aim is to find the most eligible visualization to describe the YPM orientation workspace.

5.2.1. The Equivalent Angle-Axis Representation

In the Equivalent Angle-Axis Representation, a rigid body is considered to rotate about a rotation axis where rotation amount is defined with the rotation angle, θ.

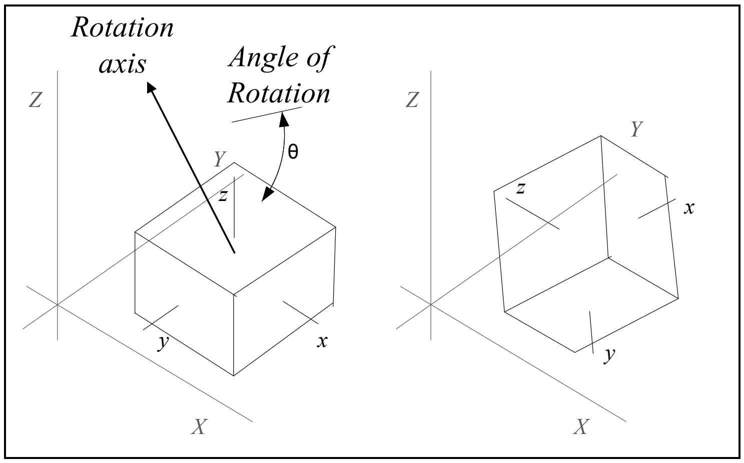

Figure 5.8. Equivelent Angle-Axis Representation

Therefore the rotation matrix, with a rotation axis $\vec{u}$, and rotation angle θ, is derived as;

$$\tilde{R}_u(\theta) = \begin{bmatrix} u_x u_x v_\theta + c_\theta & u_x u_y v_\theta - u_z s_\theta & u_x u_z v_\theta + u_y s_\theta \\ u_x u_y v_\theta + u_z s_\theta & u_y u_y v_\theta + c_\theta & u_y u_z v_\theta - u_x s_\theta \\ u_x u_z v_\theta - u_y s_\theta & u_y u_z v_\theta + u_x s_\theta & u_z u_z v_\theta + c_\theta \end{bmatrix} \quad (5.1)$$

where $c_\theta = \cos\theta$, $s_\theta = \sin\theta$, $v_\theta = 1 - \cos\theta$, and $\vec{u} = [u_x \quad u_y \quad u_z]^T$. The sign of θ is determined by the right-hand rule with the thumb pointing along the positive sense of $\vec{u}$.

There is also another way to express Equivalent Angle-Axis convention which is called exponential mapping. In this method, the rotation matrix is expressed as;

$$\tilde{R}_u(\theta) = e^{\theta u \times} \quad (5.2)$$

where x is the product operator.

In order to sweep the entire orientation workspace, the rotation axis and the rotation angle spaces are swept. The rotation axis is a unit vector and in order to sweep the unit vector space a spherical coordinate system can be used.

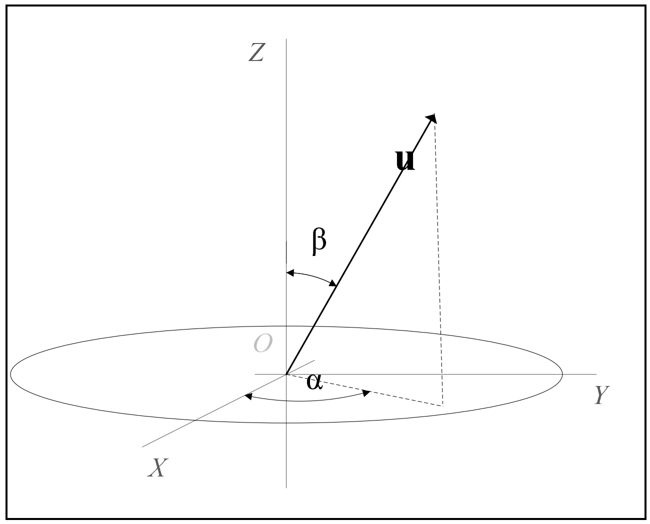

Figure 5.9. Spherical coordinate system representation of a unit vector

The unit vector in the spherical coordinate system is defined by its elevation angle (β) measured from z axis and the azimuth angle (α) measured from y axis to its orthogonal projection on x-y plane where β is $0\ to\ \pi$, α is $-\pi\ to\ \pi$ and θ is $0\ to\ 2\pi$ (magnitude of unit vectors is equal to 1). Therefore the rotation axis is expressed as;

$$\vec{u} = \begin{bmatrix} sin\,\beta\ cos\alpha \\ sin\beta sin\alpha \\ cos\beta \end{bmatrix} \tag{5.3}$$

When the rotation angle range is defined as $0\ to\ 2\pi$, it is clear that some rotation matrices are repeated. This situation causes a repetition of several orientations in the orientation space. In such a case, the represented orientation workspace may not be faithful. Probably the volume of the orientation workspace gets larger and there is no chance to analyze the workspace properly. For instance, a rotation axis with a 2π rotation angle range repeats itself with the rotation axis in opposite direction as shown in Figure 5.10.

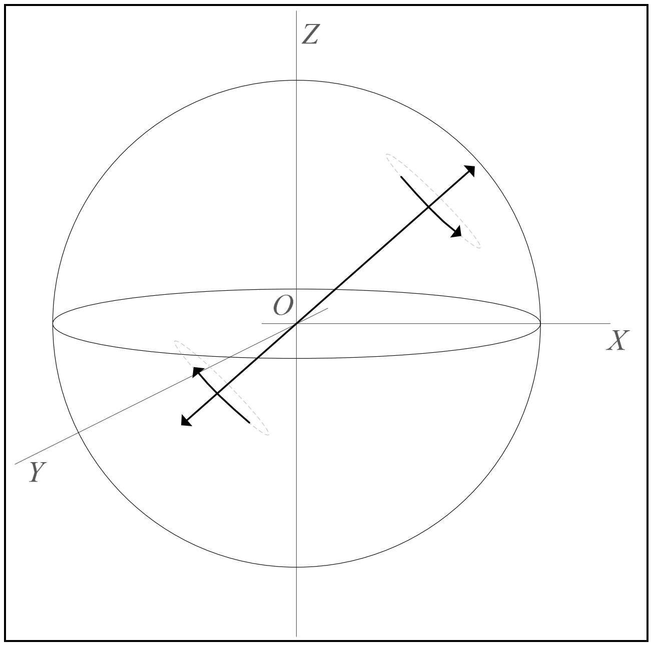

Figure 5.10. An example of rotation parameters that gives same the same orientation

The simplest example of this case is the rotation about z axis and negative z axis. The rotation about the z axis with $\pi/2$ rad actually can be achieved with the rotation about negative z axis with $-\pi/2$ rad. Therefore the couples of the rotation axes should not be represented. As a result, only a hemisphere ($z \geq 0$) is to be swept.

5.2.2. Rodrigues Parameters

A result from linear algebra known as Cayley's formula for orthonormal matrices states that for any proper orthonormal matrix, $\tilde{R}$, there exists a skew-symmetric matrix, $\tilde{S}$, such that,

$$\tilde{R} = \left(I_3 - \tilde{S}\right)^{-1}(I_3 + \tilde{S}) \tag{5.4}$$

where I_3 is a three by three identity matrix. Consequently a three dimensional skew-symmetric matrix is specified by three parameters (s_x,s_y,s_z) as;

$$\tilde{S} = \begin{bmatrix} 0 & -s_z & s_y \\ s_z & 0 & -s_x \\ -s_y & s_x & 0 \end{bmatrix} \tag{5.5}$$

These three parameters are called Rodrigues Parameters, also known as Gibbs vector. The relation between the Rodrigues Parameters and Equivalent Angle-Axis Representation [20] is

$$\begin{bmatrix} s_x \\ s_y \\ s_z \end{bmatrix} = tan\left({}^{\theta}/_{2}\right) \begin{bmatrix} u_x \\ u_y \\ u_z \end{bmatrix} \tag{5.6}$$

5.2.3. XYZ Fixed Angles

Another method of describing the orientation of a frame {B} is as follows; Start with the frame coincident with a known reference frame {A}. First rotate {B} about X_A by an angle γ, then rotate about Y_A by an angle β, and then rotate about Z_A by an angle α.

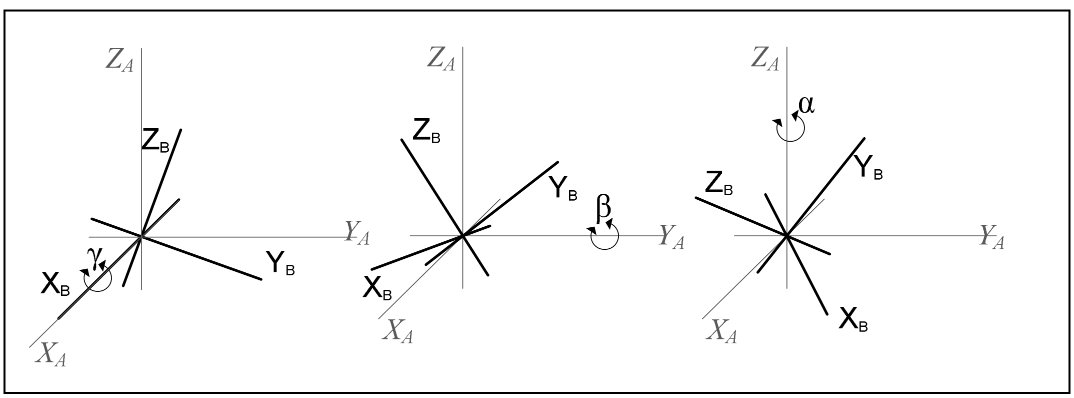

Figure 5.11. Illustration of the rotations with respect to XYZ Fixed Angles

Each of the three rotations takes place about an axis in the fixed reference frame, {A}. This convention is called as XYZ fixed angles. The word “fixed” refers to the fact that the rotations are specified about the fixed (i.e., non-moving) reference frame shown in Figure 5.11. Sometimes this convention is referred to as roll, pitch, yaw, angles.

The derivation of the equivalent matrix ${}^A_B R_{XYZ}(\gamma, \beta, \alpha)$ is straightforward because all rotations occur about axes of the reference frame;

$$ {}^A_B\tilde{R}_{XYZ}(\gamma, \beta, \alpha) = \tilde{R}_Z(\alpha)\tilde{R}_Y(\beta)\tilde{R}_X(\gamma) \tag{5.7} $$

and exponential mapping can be used to calculate this derivation. Therefore, the derivation of the rotation matrix is;

$$ {}^A_B\tilde{R}_{XYZ}(\gamma, \beta, \alpha) = e^{\alpha e_3 \times} e^{\beta e_2 \times} e^{\gamma e_1 \times} \tag{5.8} $$

where

$$ e_1 = [1 \quad 0 \quad 0]^T \tag{5.9} $$

$$ e_2 = [0 \quad 1 \quad 0]^T \tag{5.10} $$

$$ e_3 = [0 \quad 0 \quad 1]^T \tag{5.11} $$

are general unit vectors.

The parameters α, β, γ are the Euler angles.

5.3. VISUALIZATION OF ORIENTATION THE WORKSPACE

The orientation workspace differs from the translational workspace when visualization is considered. Although the translational workspace is visualized easily in the Cartesian space, the rotation space is not a simple space. Human brain has difficulties forming a picture of the orientation space. Cartesian space representations of the orientation space are tough to understand and analyze.

Even if an orientation workspace can be illustrated individually, it is hard to show the orientation workspaces at different positions together. For every reachable position in the translational workspace an orientation workspace exists as mentioned before. In such a case, the matter is to show the orientation workspaces in the translational workspace. The combination of the both workspaces is a six dimensional space but human mind can only imagine three dimensional spaces. Therefore the orientation workspaces should be analyzed at every position. In this manner, the most eligible visualization has to be investigated to analyze the orientation workspace.

In this study, an algorithm is developed to visualize the orientation workspace with various plot types. For a given position and dimensional configuration the algorithm scans the entire orientation space and saves the doable orientations. The inverse kinematic solution is used to check whether solution exists or not. In order to get a more general solution, slider limitations are not considered for all visualizations. Without any slider limitations, some features of the orientation workspace can be easily recognized such as symmetry, kinematic circuits, and so on.

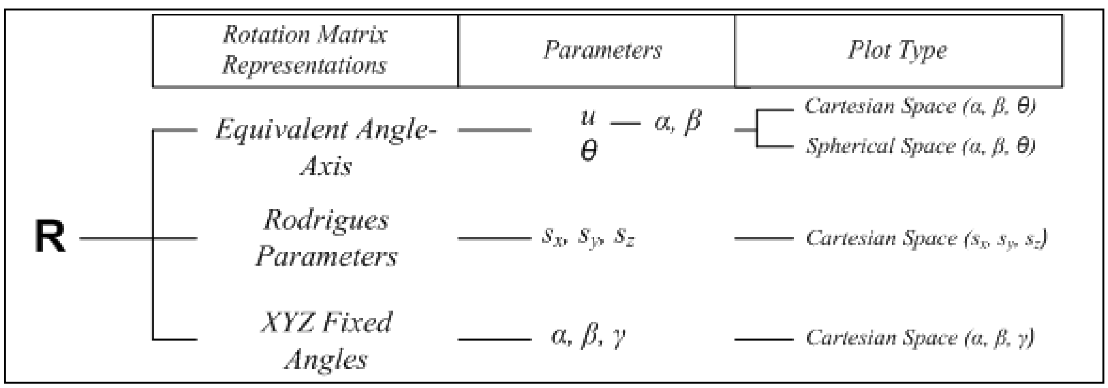

Figure 5.12. Orientation space visualization diagram

Figure 5.12 demonstrates the visualization processes in this study. The first representation of the rotation matrix is Equivalent Angle-Axis method. In this method, the rotation matrix parameters are plotted in two different ways. The first one is the general Cartesian space illustration. In the second plot the parameters are defined in spherical coordinate system: α, β are the azimuth and the elevation angles again as defined in Figure 5.9, and θ is the magnitude of the position vector.

5.3.1. Visualization of Equivalent Angle-Axis Representation

In order to sweep the full orientation space, the rotation matrix parameters have to be swept for each visualization type. In this case the parameters ranges are defined: β is $-\pi/2$ to $\pi/2$, α is 0 to π and θ is 0 to 2π, to sweep a hemisphere, as shown in Figure 5.10.

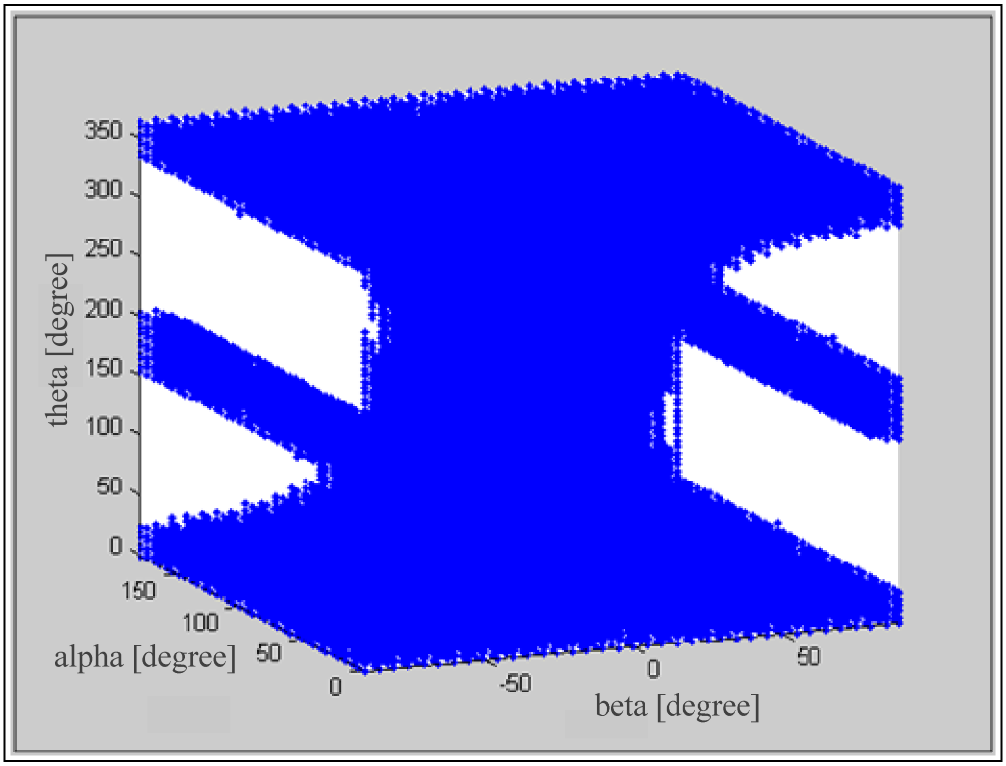

Figure 5.13. Cartesian plot of Equivalent Angle-Axis Representation

The algorithm is run for the position of the platform is $\vec{P} = [0 \quad 0 \quad 100]^T$ in mm and the dimensional configuration is; $R_B = 125$ mm, $\rho = 50$ mm and $L = 125$ mm. The result is shown in Figure 5.13. In this search doable orientations are represented with blue dots. It is observed that there is no change along the α axis. It means that orientation workspace can be studied in β-θ plane, instead of 3D visualization.

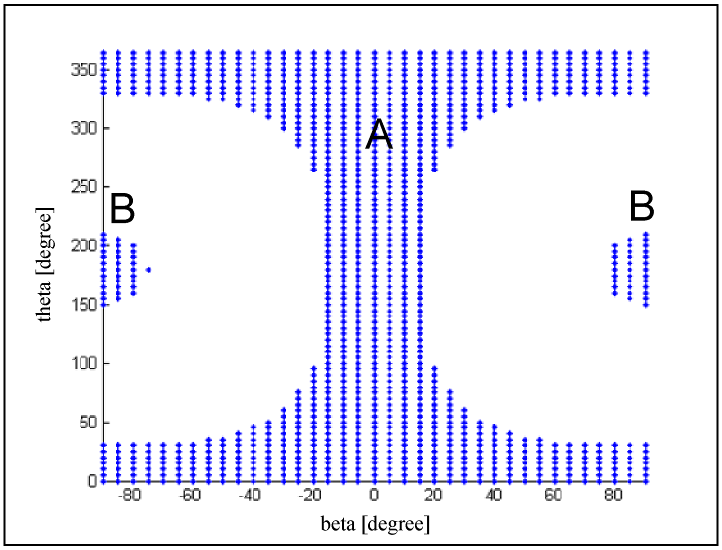

Figure 5.14. 2D plot of Equivalent Angle-Axis Representation (α=0, plane)

It is obvious that, the plane view of the Figure 5.13 has two kinematic circuits, A and B. It means that the YPM has two different circuits, and two assembly modes. The first and last columns in Figure 5.15 represent the rotation about x axis where β is equal to $\pi/2$, $-\pi/2$ and α is $\pi/2$, shown in Figure 5.15.

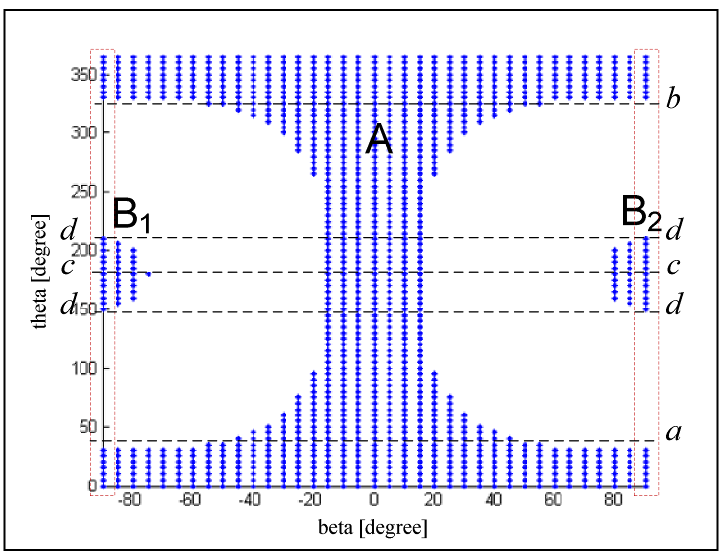

Figure 5.15. A detailed view of Equivalent Angle-Axis Representation (α=90, plane)

Let's start with β equal to 90 degree and θ equal to 0 case. Because θ is 0, there is no rotation and this orientation represents the default orientation of the platform. When θ is 35 degree at that column, the platform reaches its maximum rotation about x axis. Similar to θ is zero case when θ is 360 degree the platform is in the default orientation (no rotation). Therefore, it is expected that platform can rotate 35 degree about x axis in opposite direction. This case can also be seen at the top of that column (*a*, *b* in Figure 5.15). These examples agree with the first circuit which is A.

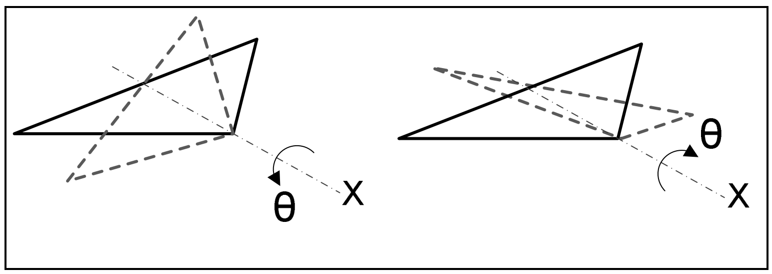

Figure 5.16. Rotations about x axis and in opposite direction

When θ is 180 degree, the orientation exactly represents the flipped platform orientation where inverse kinematic solution is possible, shown in Figure 5.17. However it is impossible to do this orientation because the maximal rotation about x axis is 35 degree. If the manipulator is disassembled, and reassembled with a flipped platform, this solution becomes possible. This exactly represents the assembly modes of the YPM. According to this, if the YPM is started with second assembly mode, the maximum rotation about x is also expected as 35 degree. This situation can be observed when the maximum rotations of circuit B is searched (*d* in Figure 5.15).

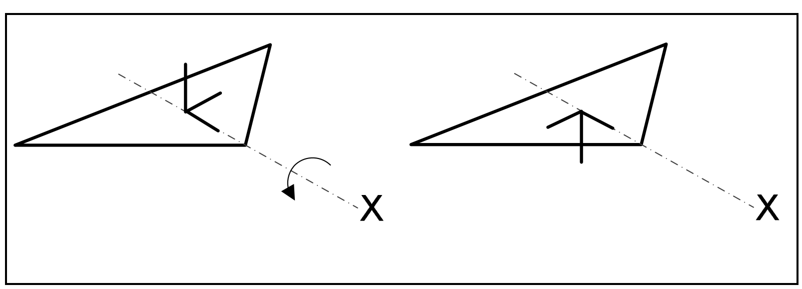

Figure 5.17. The flipped platform case

The first column is actually same as the last column. When β is -90 degrees where α is zero, the platform rotates about the negative x axis. The 35 degree rotation about x axis and -35 degrees about negative x axis will give the same orientation. Therefore B_1 and B_2 are connected in rotation space and they complete each other which give region B.

According to this result, in order to get a proper visualization, Figure 5.14 has to bend about axis I to connect line 1 and line 2, shown in Figure 5.18. On the other hand it has to also bend about axis II to connect line 3 and line 4. This creates a complicated surface that it is difficult to understand.

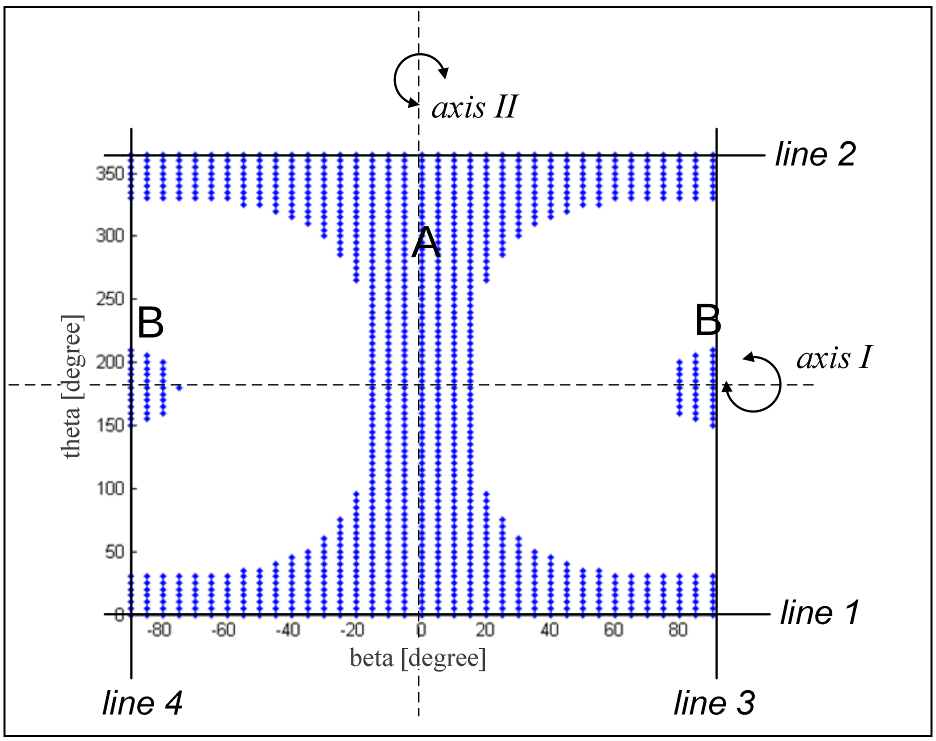

Figure 5.18. Description of complicated surface of Figure 5.14

The geometrical features of B_1 and B_2 are close but different. It indicates that the orientation workspace along the α axis is not same. Therefore, study of the orientation workspace by slicing the 3D plot is impractical. In order to see the effect of the α, several α planes has to be studied together.

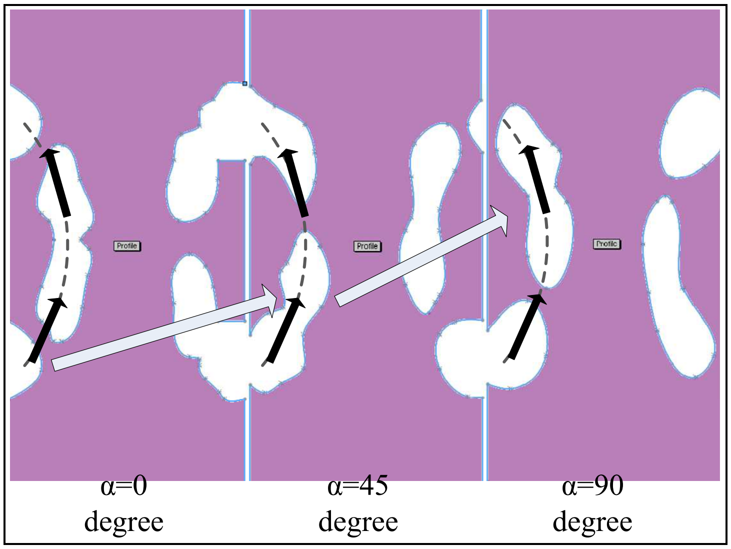

Figure 5.19. Illustration of the several α planes

Another dimensional configuration is set with the same position of the last example. It is observed that the unreachable regions narrow in Figure 5.19. Their geometric features also seem to be changed. They look like beans now. As α changes, the bean gaps spins along the α axis and transforms to another shape The gap whose head is only seen at first plane becomes an entire body and gets lost after a while.

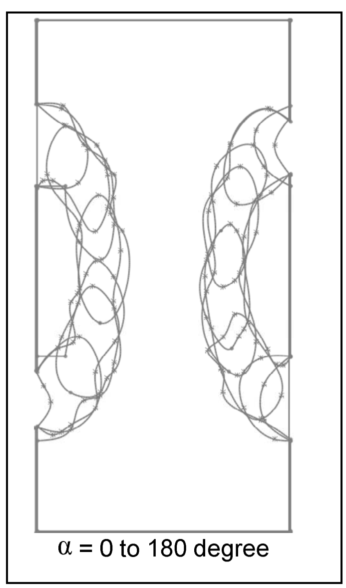

Figure 5.20. Another demonstration of Equivalent Angle-Axis representation

A new illustration is performed as shown in Figure 5.20. In Figure 5.20, all planes are added to the back of the each other and an image is created from the front view. It is an excellent representation of the complexity of the orientation workspace in Equivalent Angle-Axis representation. While the gaps are spinning, the plane views bend. Therefore it is impossible to determine the kinematic circuits where they are nested. In such a case it is unfeasible to predict the size of the workspace since the circuits cannot be recognized. Another visualization technique has to be developed instead of working with this unfaithful visualization.

A second method is to plot the orientation workspace in a spherical coordinate system. In this manner, α and β are the azimuth and the elevation angles again as defined in Figure 5.21 (a) and θ is the magnitude of the position vector.

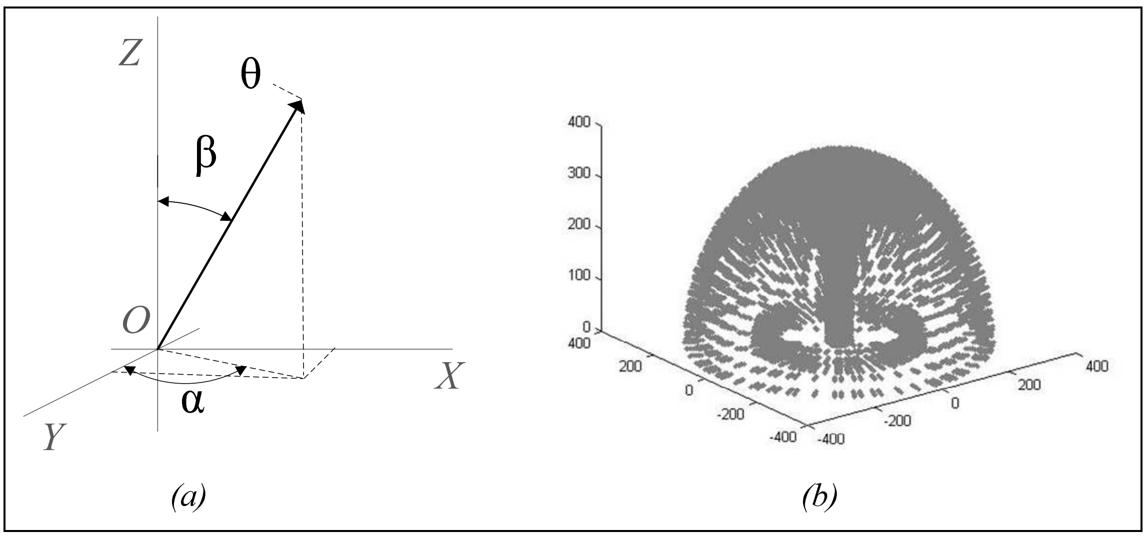

Figure 5.21. (a) Illustration of definition, (b) 3D spherical coordinate system plot of Equivalent Angle-Axis Representation

By definition, α and β set the direction of the rotation vector and θ sets the magnitude of the vector, where θ actually represents the rotation amount. In Figure 5.22 (b) a detailed view of the Figure 5.21 (b) is shown. In this figure a slice of the orientation workspace is illustrated to analyze the circuits. There is an umbrella and a ring in the figure, which are not connected.

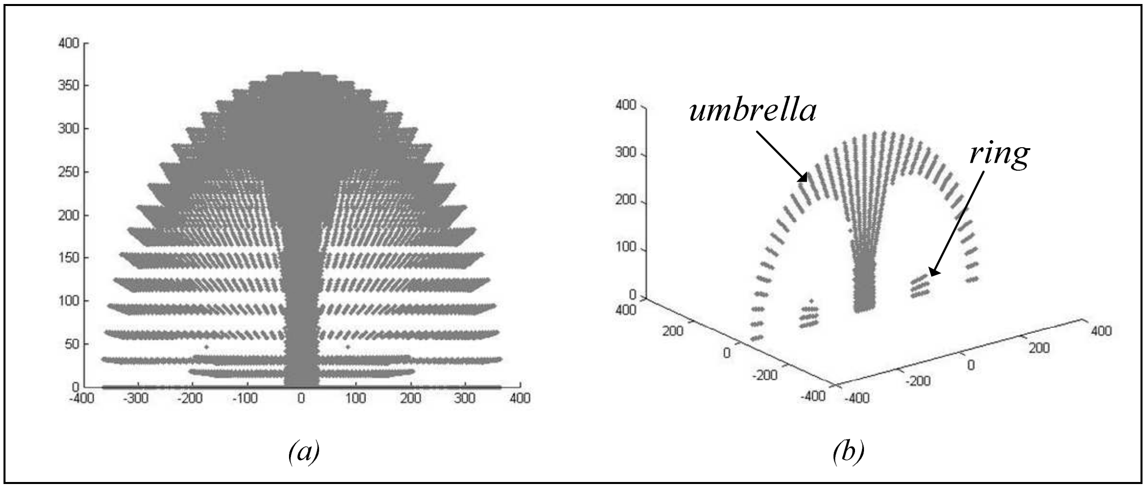

Figure 5.22. (a) X-Z view of the Figure 5.21 (b), (b) $\alpha = 0$ slice

These two objects represent the circuits of the workspace. Similar to Equivalent Angle-Axis method, the circuits are complex and it is hard to say which circuit the manipulator is in. In this condition a proper search on the orientation workspace size is unfeasible. It is an undesirable situation to analyze the shape of the workspace. Therefore, this visualization is stated as another unfaithful approach to calculate the orientation workspace size.

5.3.2. Visualization of Rodrigues Parameters

The orientation workspace is plotted in Cartesian space using Rodrigues Parameters, as shown in Figure 5.23. When the definition of Rodrigues Parameters is considered, the axes in Cartesian plot cannot be named. In equation 5.6, the parameters are related with the rotation axis and the rotation amount. Actually it is too complicated to make sense of the visualization of these parameters. In addition, the kinematic circuits cannot be recognized. In this manner Rodrigues Parameters Representation is not a suitable method when the evaluation of workspace size is considered. Therefore this representation is eliminated.

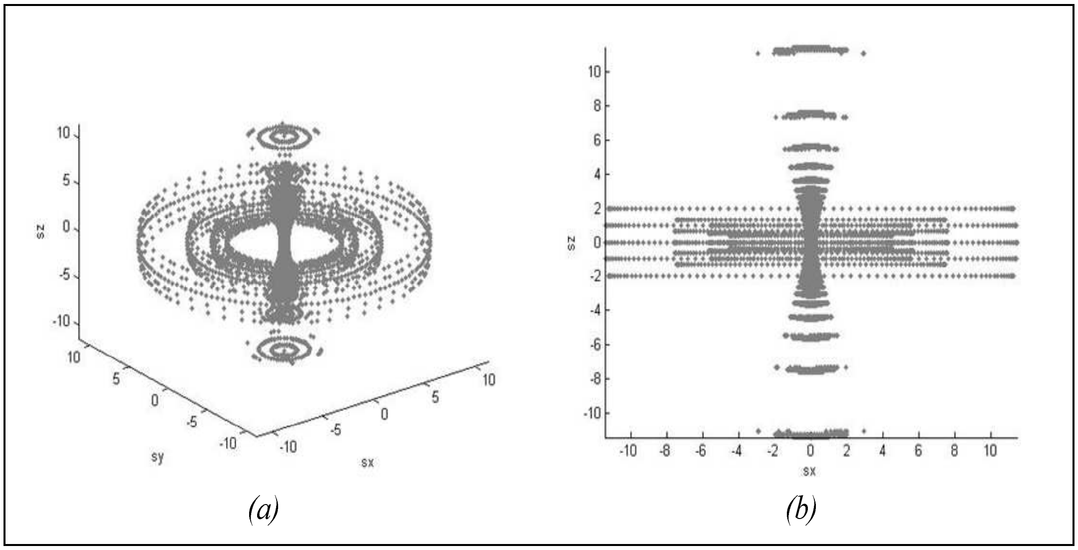

Figure 5.23. Cartesian plot of Rodrigues Parameters

5.3.3. XYZ Fixed Angles Representation

In this representation the parameters are defined as; γ is $-\pi\ to\ \pi$, β is $-\ \pi\ to\ \pi$, and α is $-\pi\ to\ \pi$ where these angles represent the rotations about global frame x axis, y axis and z axis respectively. The result is plotted in the Cartesian space, as shown in Figure 5.24.

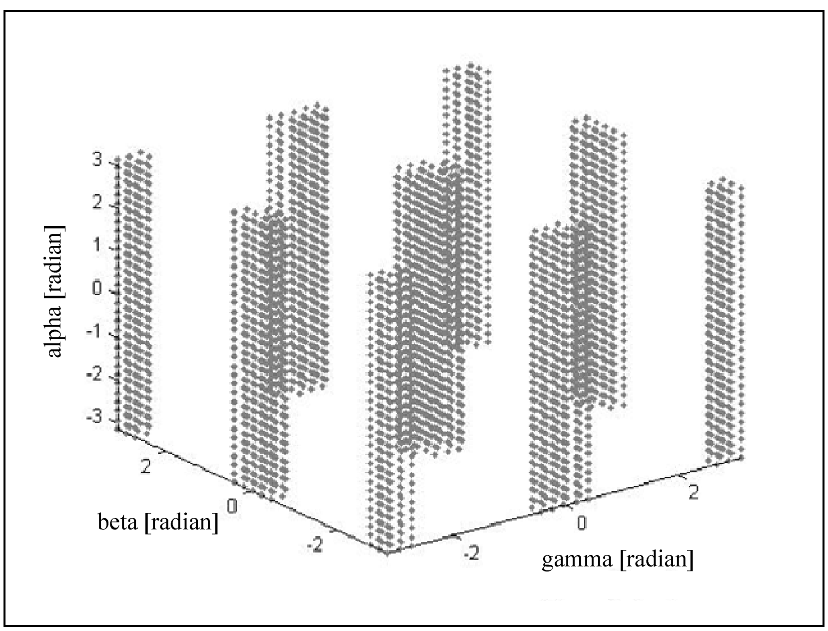

Figure 5.24. XYZ Fixed Angles visualization

There are nine objects in the solution which are one entire, four half and, four quarter bars. The sizes and geometric features of the bars seem to be similar. Therefore these solution sets could be the circuits of the manipulator. There is no doubt the middle bar represents the default orientation of the platform. It can be easily understood that when there is no rotation (all angles are zero), the platform is in the default orientation. This orientation is named as identity orientation and its circuit is named as identity circuit. That is because when the platform is in its default orientation its rotation matrix is an identity matrix. It is obvious that there is no change along the z axis. In this manner, the orientation workspace can be studied in xy plane, as illustrated in Figure 5.25.

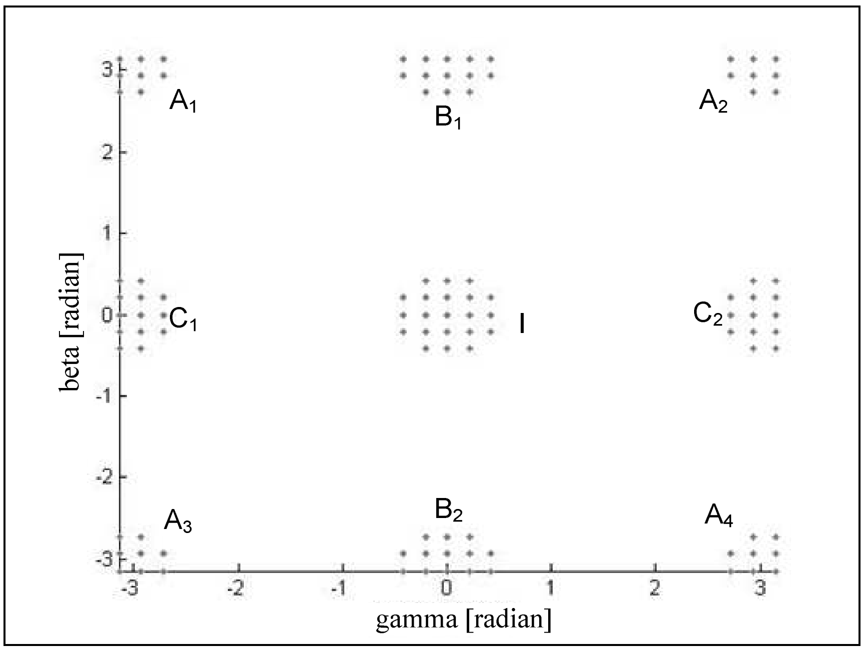

Figure 5.25. X-Y view of Figure 5.24

It is obvious that rotation about an axis with π and $-\pi$ radian gives the same orientation as shown in Figure 5.26. According to this rotation about y axis with $-\pi$ is equal to rotation about y with π radian. Similar to this, rotation about x axis with $-\pi$ and π radian are equivalent also. Region A_1 represents the rotation about x axis with $-\pi$ and then about y with π radian. A_2 represents the rotation about x axis π and then rotation about y axis with π radian. Therefore A_1 and A_2 are the same orientations. In this manner A_3 and A_4 are also same and furthermore they also give the same orientation with A_1 and A_2

group. It indicates that the A_1, A_2, A_3, and A_4 are connected in rotation space and totality of them seems to represent a kinematic circuit. However this orientation can be reached from the identity circuit by rotation about z axis as proved in Figure 5.27.

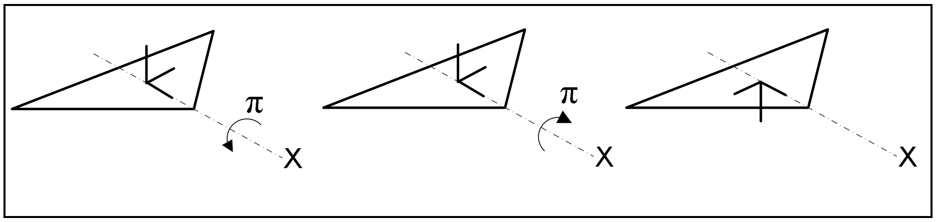

Figure 5.26. Rotation about x axis π and –π radian

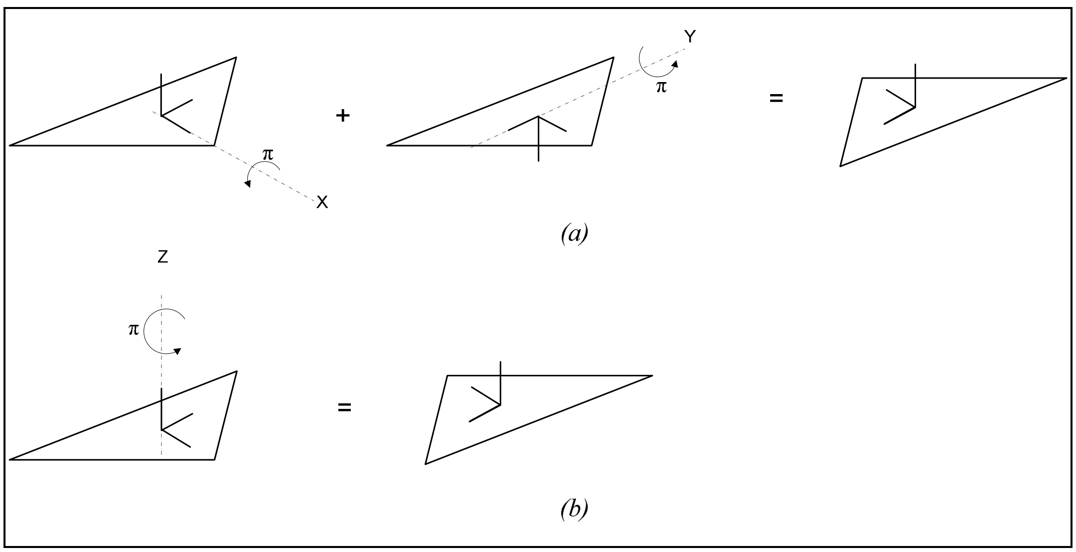

Figure 5.27. (a) Rotation about x and y axes with π radian. (b) Rotation about z axis with π radian

It shows that circuit A is included by identity circuit. In order to get a faithful orientation workspace size calculation, any orientation should not to be represented more than once. It means that the rotation space where circuit A is included can be cancelled.

Similar to A_1 and A_2 regions, the regions of C_1 and C_2 are connected and represent another circuit. However the orientations in circuit C are not included by the identity circuit. Figure 5.28 shows that the circuit C exactly represents the flipped platform case.

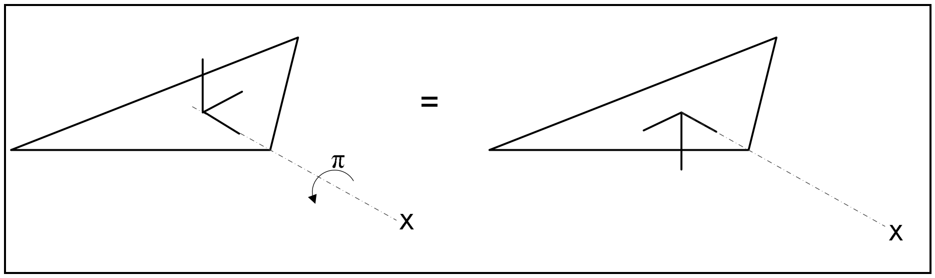

Figure 5.28. The circuit C represents the flipped platform case

In addition to that circuit B orientations can be reached by circuit C using the rotations about z axis as shown in Figure 5.29.

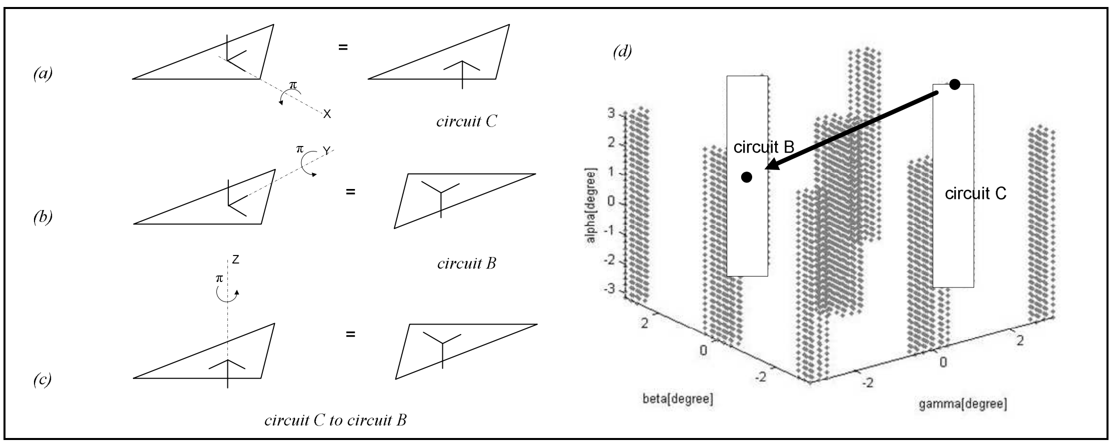

Figure 5.29. (a) Circuit C. (b) Circuit B. (c) Circuit C to circuit B with a π rotation about z axis. (d) Visualization of (c) in Figure 5.24

Therefore circuits B and C represent the same circuit. An orientation workspace including the identity circuit and circuit C (or B) is desired to represent the entire orientation space. In this manner the ranges of the rotation angles should be considered again.

It is obvious that the orientations are more comprehensible in Equivalent Angle Axis Representation and there is no repetition in the orientation space. An approach is developed to verify the results above. In this approach rotation matrices are created in Equivalent Angle-Axis representation and the orientation workspace is plotted in XYZ Fixed Angles. Therefore the question is the investigation of the matrix parameters for a given rotation matrix. The inverse problem was studied by Craig [21]. The total rotation matrix can be obtained by the multiplication of each axis rotations in a given order.

$$\tilde{R}_{XYZ}(\gamma, \beta, \alpha) = \tilde{R}_Z(\alpha)\tilde{R}_Y(\beta)\tilde{R}_X(\gamma) \tag{5.12}$$

$$\tilde{R}_{XYZ}(\gamma, \beta, \alpha) = \begin{bmatrix} c\alpha c\beta & c\alpha s\beta s\gamma - s\alpha c\gamma & c\alpha s\beta c\gamma + s\alpha s\gamma \\ s\alpha c\beta & s\alpha s\beta s\gamma + c\alpha c\gamma & s\alpha s\beta c\gamma - c\alpha s\gamma \\ -s\beta & c\beta s\gamma & c\beta c\gamma \end{bmatrix} \tag{5.13}$$

where $c\alpha = \cos\alpha$, $s\alpha = \sin\alpha$, etc.

$$\tilde{R}_{XYZ} = \begin{bmatrix} r_{11} & r_{12} & r_{13} \\ r_{21} & r_{22} & r_{23} \\ r_{31} & r_{32} & r_{33} \end{bmatrix} \tag{5.14}$$

From Equation 5.14, we see that, by taking the square root sum of the squares of r_{11} and r_{21}, we can compute $\cos\beta$. Then, we can solve for β with the arc tangent of $-r_{31}$ over the computed cosine. Then, as long as $c\beta \neq 0$, we can solve for α by taking the arc tangent of $r_{21}/c\beta$ over $r_{11}/c\beta$ and we can solve for γ by taking the arc tangent of $r_{32}/c\beta$ over $r_{33}/c\beta$.

In summary,

$$\beta = atan2(-r_{31}, \sqrt{{r_{11}}^2 + {r_{21}}^2}) \tag{5.15}$$

$$\alpha = atan2(r_{21}/c\beta\,, r_{11}/c\beta) \tag{5.16}$$

$$\gamma = atan2(r_{32}/c\beta\,, r_{33}/c\beta) \tag{5.17}$$

where $\mathrm{atan2}(y, x)$ is a two-argument arctangent function.

Although a second solution exists, by using the positive square root in the formula for β, we can always compute the single solution for which $-90.0° \leq \beta \leq 90.0°$. This is usually a good practice, because it can then define one-to-one mapping functions between various representations of orientation. However, in some cases, calculating all solutions is important. If $\beta = \pm 90.0°$ (so that $\cos\beta = 0$), the solution of (4.18) degenerates. In these cases, only the sum or the difference of α and γ can be computed. One possible convention is to choose $\alpha = 0.0°$ in these cases, which has results given next.

If, $\beta = 90.0°$ then a solution can be calculated to be

$$\begin{aligned} \beta &= 90.0° \\ \alpha &= 0.0° \\ \gamma &= atan2(r_{12}, r_{22}). \end{aligned} \tag{5.18}$$

If, $\beta = -90.0°$, then a solution can be calculated to be

$$\begin{aligned} \beta &= -90.0° \\ \alpha &= 0.0° \\ \gamma &= -atan2(r_{12}, r_{22}). \end{aligned} \tag{5.19}$$

It has been proven before the rotation axis and its opposite direction vector creates the same orientation in Section 5.2.1. . In these ranges, it is also observed that the rotation vectors on xy plane have couples, shown in Figure 5.30. In order to avoid repetition of some orientations, the half of the x-y plane circle should be swept.

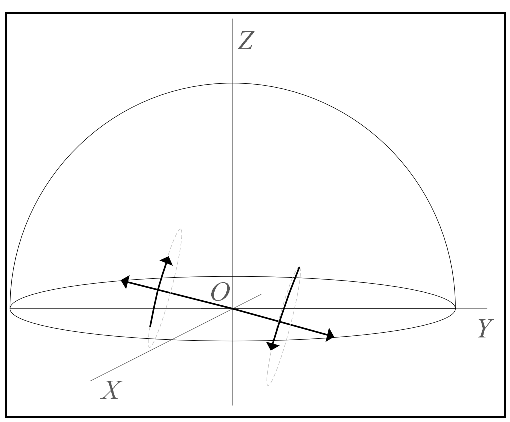

Figure 5.30. X-Y plane vectors have their couples on x-y plane in opposite direction

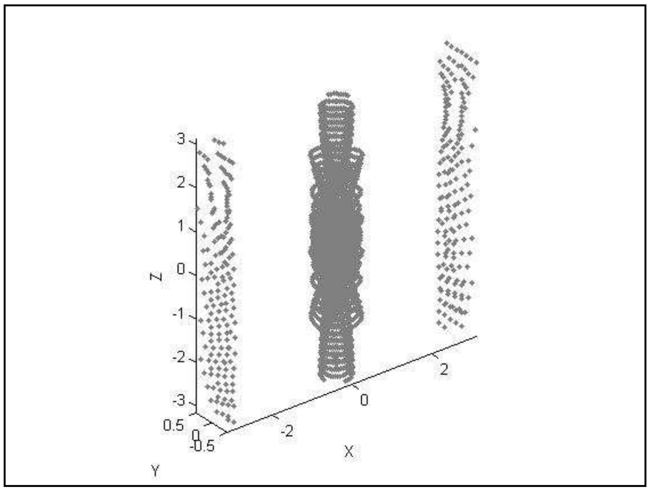

Figure 5.31. Orientation workspace in XYZ Fixed Angles

With this new range the result is shown in Figure 5.31. The result is as expected before. There are two cylindrical bars which are identity circuit and flipped platform circuit. The flipped platform circuit points seem to be sparse. Another result with higher resolution explains this, shown in Figure 5.32.

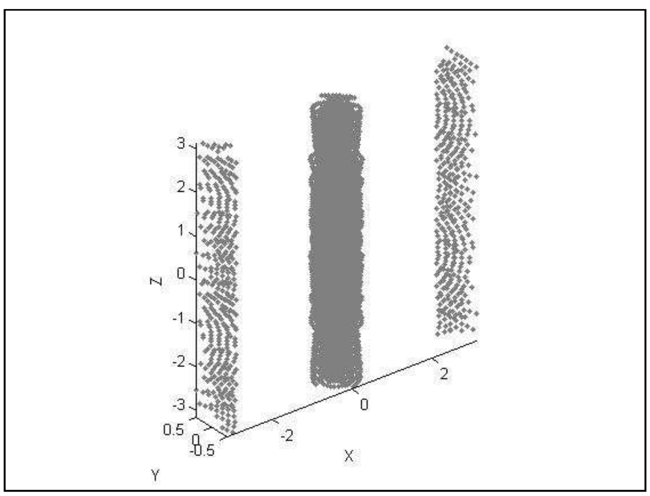

Figure 5.32. Orientation workspace in XYZ Fixed Angles with a higher resolution

The distance between solutions is getting separated while moving away from the origin. It means that the stepsize is changing through the boundaries where it is actually constant in Equivalent Angle-Axis Representation. That is because the rotation matrices are generated in Equivalent Angle-Axis Representation but plotted in XYZ Fixed Angle. In other words, the orientations are generated in spherical coordinate space and transformed to Cartesian space for visualization and this transformation causes varying stepsize according to position of the solution.

The feature of XYZ Fixed Angles representation explains trends of the solution along the z axis. Remember that the rotations starts with x axis and continues with y axis. After these rotations are done platform can rotate about z axis freely. The boundaries of the solutions are determined by the rotation about x and y axes. This is caused by the state of no slider range limitation. After the platform reaches an orientation, sliders can draw circles on the base plane and each slider changes its position with the other one while position of the platform remains constant, as demonstrated in Figure 5.33.

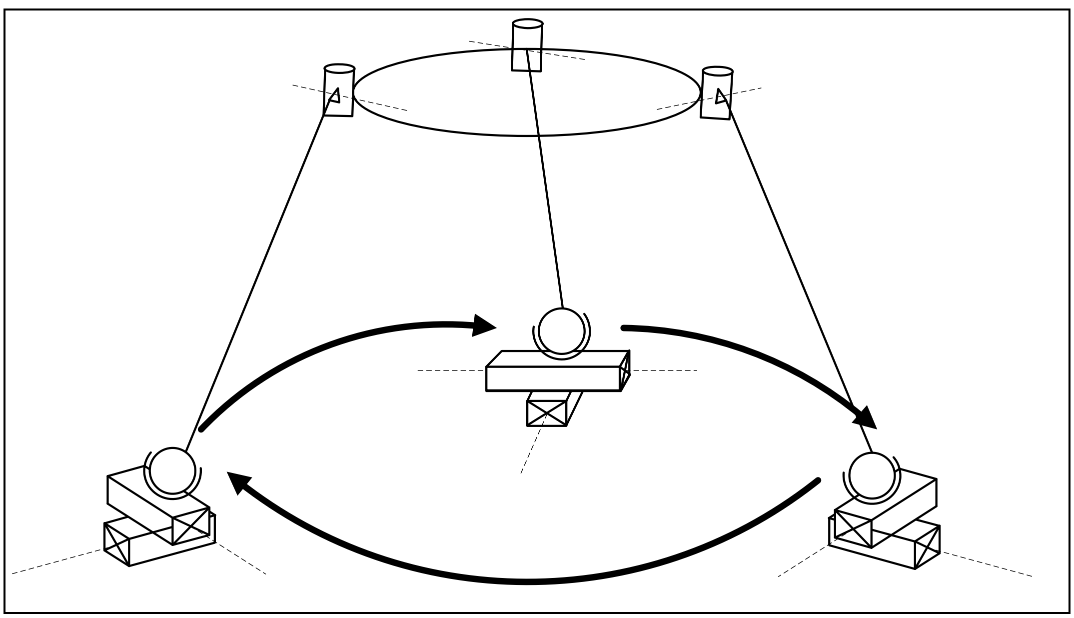

Figure 5.33. Z rotations with constant x-y orientation of the manipulator

After z is eliminated, the orientation workspace has become a plane problem which is more efficient for the calculations and makes the algorithm shorter. It is observed that the plane shapes of the bars do not remain circular. It transforms to another shape and, the circuits are connected when dimensional configuration is changed, as illustrated in Figure 5.34.

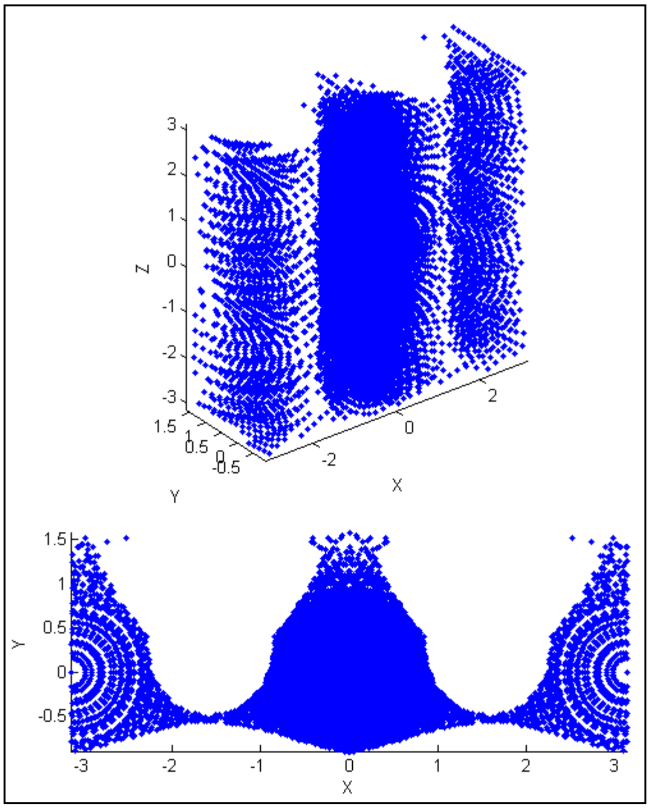

Figure 5.34. Orientation workspace of a different configuration

As a summary, XYZ Fixed Angle Representation is found as the most suitable visualization to implement the orientation workspace. By the help of Equivalent Angle-Axis convention it is realized that the rotation angle ranges are $-\pi$ to π for the x axis and $-\pi/2$ to $\pi/2$ for the y axis where the rotations about the z axis are ignored. After that, the rotation matrices can be created with XYZ Fixed Angle representation. It is observed that the whole orientation space is scanned while the rotation angles are swept in those ranges. In addition, it is found that the orientation space can be represented in two dimensional Cartesian space and the orientation capability of the different configurations can be evaluated by the area of this two dimensional workspace.

6. OPTIMIZATION OF THE WORKSPACE

The workspace of the manipulator is the combination of both translational and orientation workspaces as mentioned before. The question is what makes a workspace optimum or how a workspace is made optimal. By the definition of the maximal workspace, maximal orientation workspaces are desired for every point of translational workspace. But remember that micromachining manipulator tasks in translation are in micron level and also it is realized that it is actually one dimensional, as mentioned at Section 5.1. . Therefore the orientation capability of the platform in this miniature range becomes more important. The capability of orientation for a specified platform position can be measured with the area of the orientation workspace in XYZ Fixed Angles visualization, as mentioned before. Therefore the sum of those areas in a specified translational range would indicate the total orientation capability.

Let's say micromachining process requires 10 mm translational range in z axis. Therefore the maximal orientation workspaces are searched in a range of 10 mm height. However the location of this range in the translational workspace z direction is not known. An example is illustrated in Figure 6.1, the maximal orientation capability of a configuration is at z_1, and the other is at z_2.

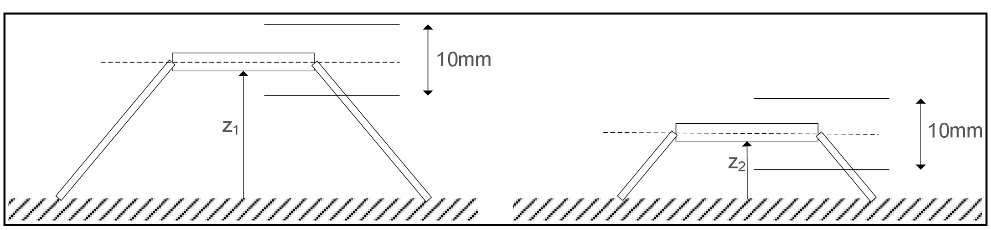

Figure 6.1. Location of maximal orientation workspaces at different configurations

A new variable "operating height" is defined and symbolized with z. The kinematic solution is parameterized again with the new variable. By this definition the platform position vector is reduced to $\vec{P} = [0 \quad 0 \quad z]^T$.

6.1. OPTIMIZATION WITHOUT SLIDER CONSTRAINTS

It is clear that without any slider range problem, the question is not the dimensions, it is the dimensional ratios. For example, if a set of dimensions are doubled, the characteristic of the manipulator remains the same. If there are some ratios that make the workspace optimum, then it can be used in the optimization with slider limitations.

Without slider limitations, R_B has no importance. The sliders can move any position on base plane. Therefore R_B is evaluated according to given z value for the inverse kinematic solution.

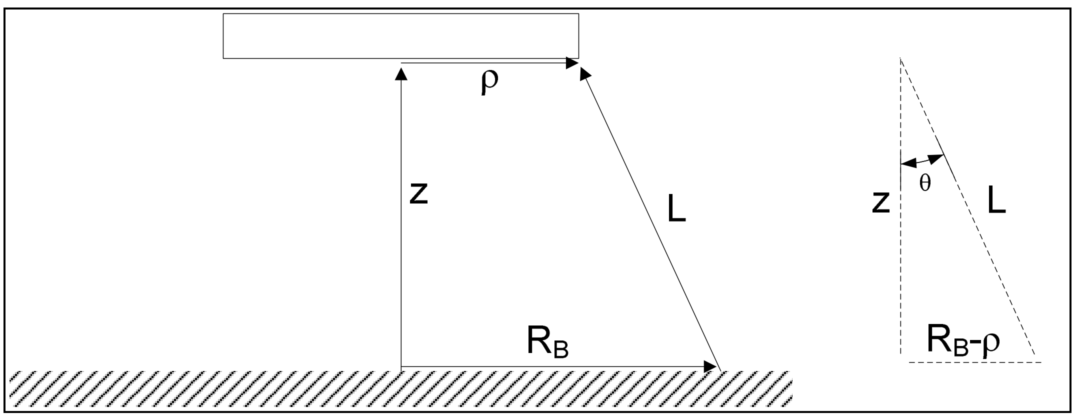

Figure 6.2. Calculation of R_B according to given z

$$\theta = cos^{-1}\frac{z}{L} \qquad (6.1)$$
$$R_B = \rho + L\sin\theta$$

A minor search is conducted for a specified z with various configurations, shown in Figure 6.3. In this search the parameters are defined as; $z = 100$ mm and $\rho = 50$ mm with various L values.

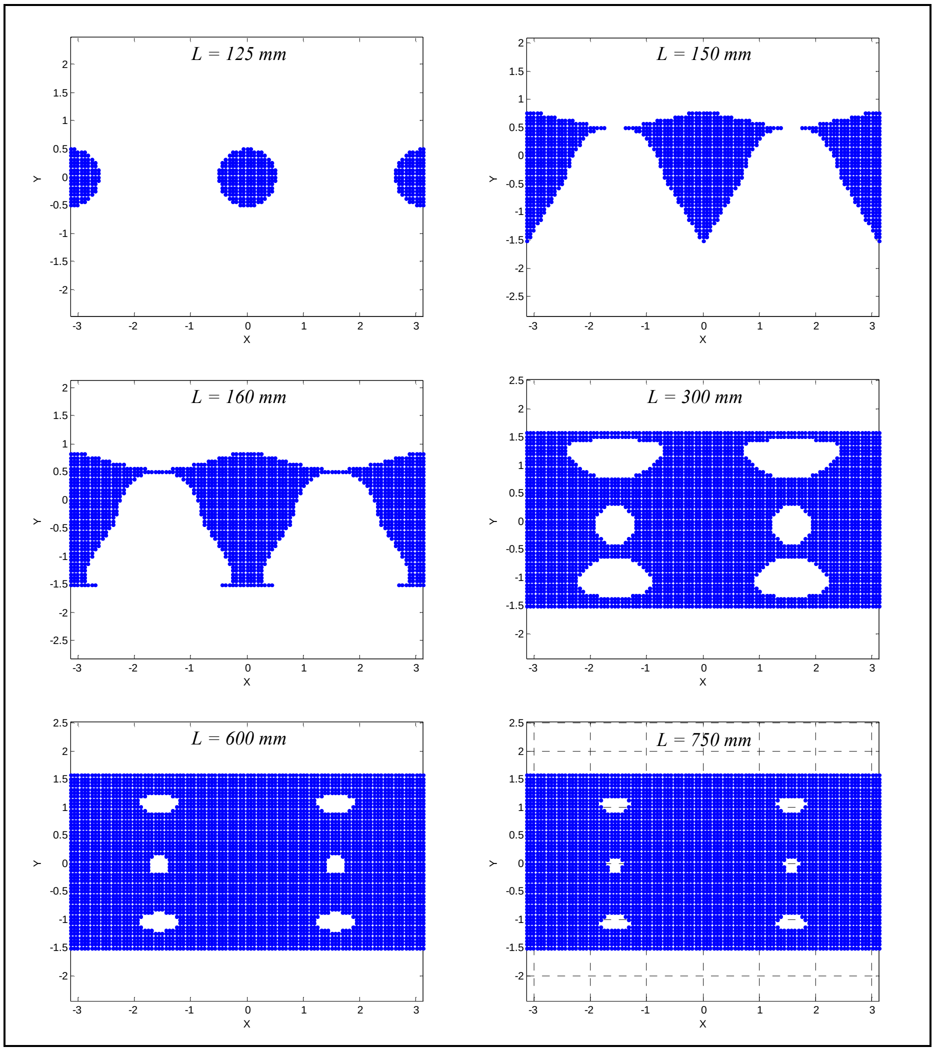

Figure 6.3. Orientation workspaces for different configurations

The region where there is no solution shrinks and become internal gaps (singularities) while L is been increasing. The singularities in the figure occur at the rotations about x $-\pi/2$, $\pi/2$ radian, and rotation about y $-\pi/3$, $\pi/3$ radian. Because of the kinematic characteristic of the manipulator, these rotations are impossible. An example of this rotation set is demonstrated in Figure 6.4. When the platform rotates about x axis by π radian, the revolute joint circle becomes parallel to the base plane. In this situation the connection of the leg and the base plane is impossible.

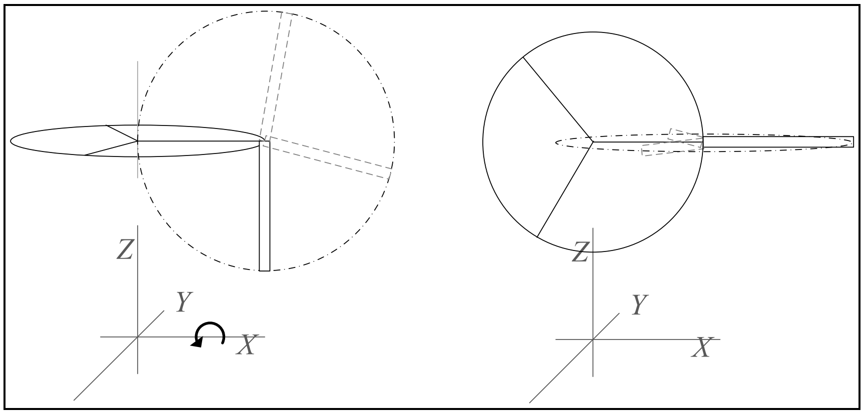

Figure 6.4. Impossible orientations of the manipulator

The circuits get connected when L is 150 mm in Figure 6.3. It is clear that there is a critical leg length value where circuits get connected. This critical value is termed as $L_{critical}$ from this moment. In these instants, two circuits get connected and the workspace size gets doubled. Therefore, it is important to recognize $L_{critical}$ values for different configurations. In this manner, an image processing algorithm is developed to identify the connection instants.

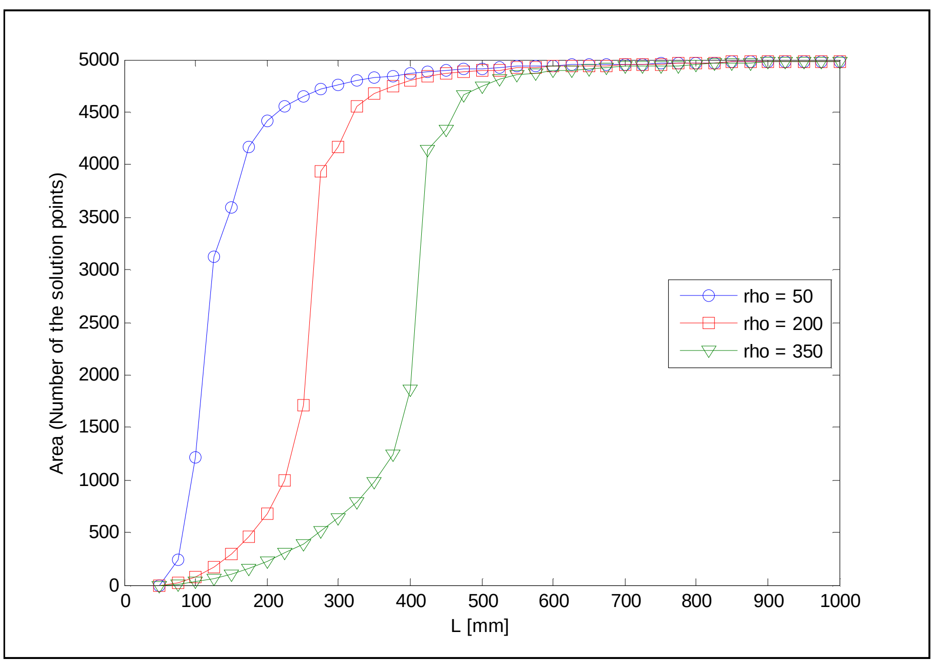

Figure 6.5. $L_{critical}$ search for different configurations

In this algorithm the 2D Cartesian space results are transformed to an image, and the algorithm tracks the boundaries of the objects in the image. After the recognition of the objects, the algorithm decides the number of the objects. The number of pixels in the boundary of an object can be assumed as the area of the object. Thus, several tests are conducted to investigate the effect of the configuration on the $L_{critical}$. In these tests z is set to 50mm and the numbers of the pixel values are computed while L, ρ values are increasing. The result is shown in Figure 6.5. The orientation workspace of the manipulator increases while L is increasing. $L_{critical}$ values can be observed where the data lines are vertical. When the radius of the platform increases, the critical length values increases. The relationship between $L_{critical}$, ρ, and z is observed as;

$$L_{critical} = \rho + z \tag{6.2}$$

As a summary, the mechanism can pass one circuit to the other one when $L_{critical}$ is exceeded. Actually YPM does not need this ability. Because the flipped platform orientation means that the workpiece would stay under the platform during the machining process.

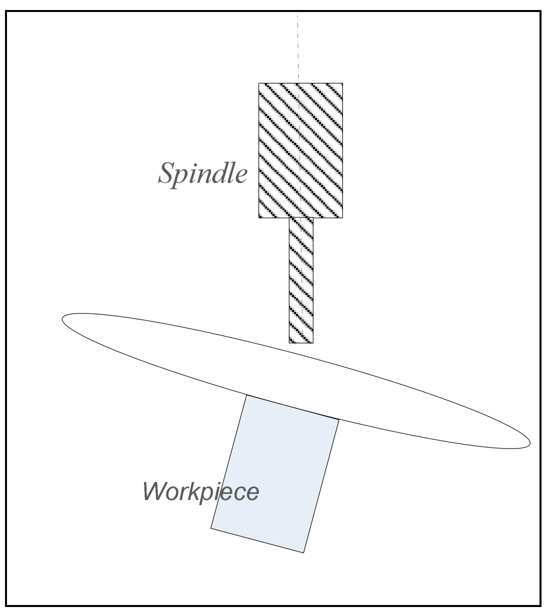

Figure 6.6. Flipped platform machining case

Therefore it is important to find the maximal identity circuit area. It is obvious that the largest boundary of the identity circuit is observed when the two circuits get connected. At this moment, another observation is the geometric features of the objects. When $L_{critical}$ values are achieved, it is seen that the features of the objects are absolutely unique for different configurations. The new question is the properties of the different features. The importance of the features has to be determined when the area of them seem to be equal.

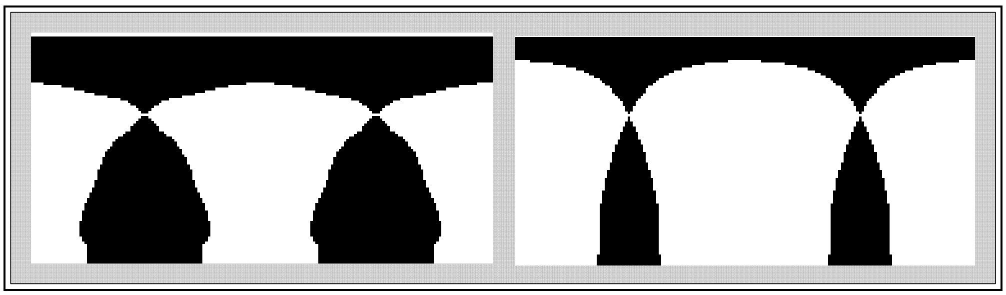

Figure 6.7. Illustration of object features for different configurations

The shortest paths from one side to other or top to bottom pass through the middle of the image. It means that the middle of the image is the most widely-used region. Therefore the middle of the figure is the most important region (default orientation) and the importance of the points decrease while the distance is increasing.

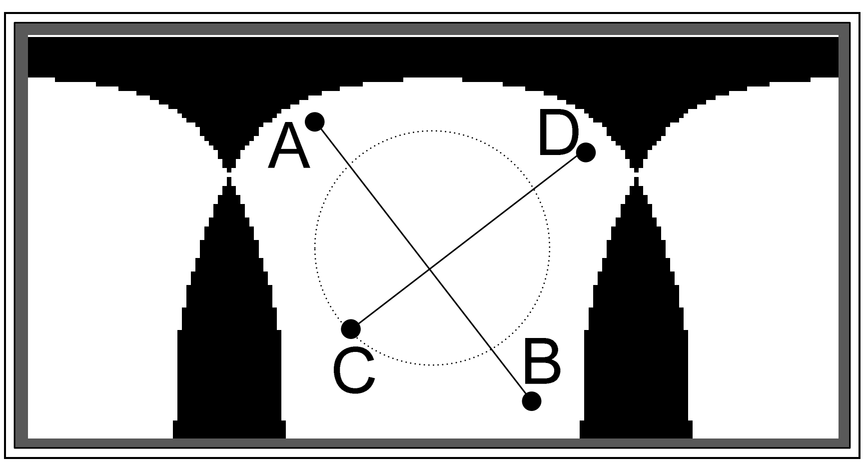

Figure 6.8. The shortest paths passing through the middle of the image

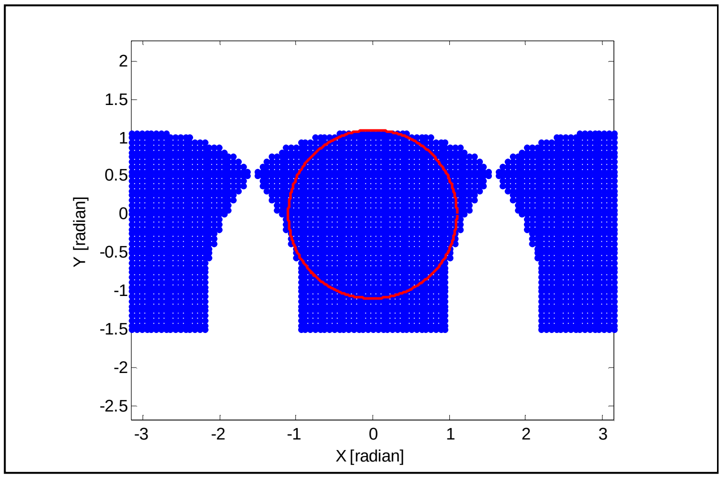

Figure 6.9. Circle fit method demonstration

Solution is to fit a circle to the middle of the figure where the circle intersects the boundary of the middle object. The rotations about x and y axes have the same importance because the rotations are directionless. A new algorithm is developed to find the radius of the circle. The algorithm increases the radius of the circle until it reaches the object boundary.

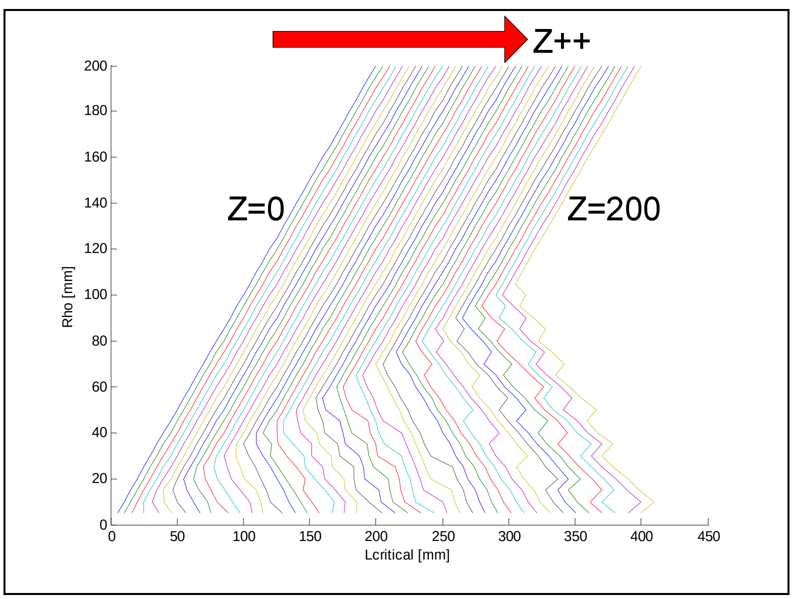

Figure 6.10. Investigation of $L_{critical}$ for various ρ and z

A search is done that represents the evaluation of the $L_{critical}$ with various z and ρ values. It is obvious that there are two regions in the figure, which are upper and lower. These two regions are separated with a specific line shown in the Figure 6.11. Let's say user wants to work in a range of z → 0 to 200 mm. When solution a_1 is chosen ρ is 105 mm and $L_{critical}$ is 305mm. For z is 100 mm and ρ is 105 mm, $L_{critical}$ is about 200 mm which is smaller than the chosen L value 305 mm. Therefore it is realized that the chosen configuration (a_1) satisfies the all $L_{critical}$ conditions in the range of z → 0 to 200 mm.

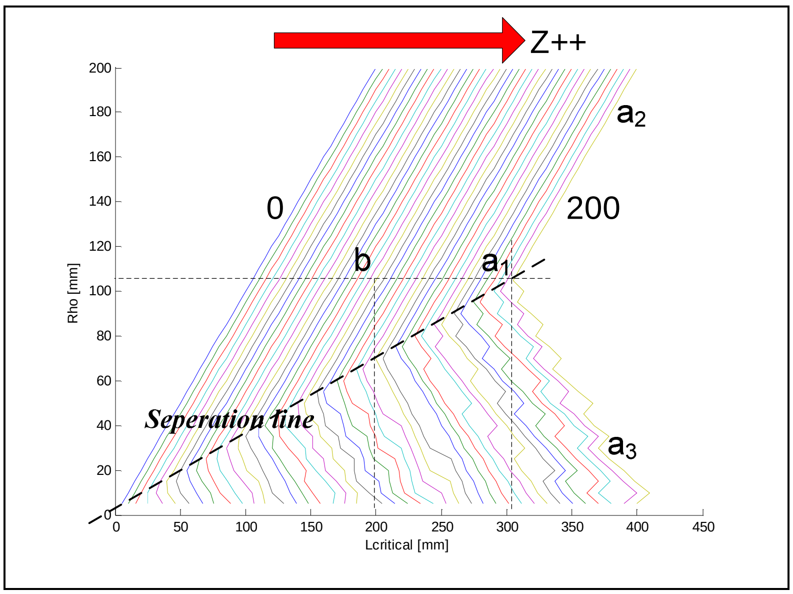

Figure 6.11. Detailed view of Figure 6.10

Another question is the eligibility of the configurations (a_1, a_2, a_3) on $z = 200mm$ line. Therefore circle fit method can be applied to find out which one provides the maximum radius. It is seen that the maximum radius of the circle is observed at the configuration $\rho = 10$ mm, $L = 409.2306$ mm, where the radius of the circle is R=1.0472 radian.

6.2. OPTIMIZATION WITH SLIDER CONSTRAINTS

The physical constraints complicate the derivation of optimality function including all variables. The existence of sharp starts and ends corrupts the continuity of the optimality function. Without slider constraints, an optimal surface can be formed where the surface equation is expressed in Equation 5.2.

Two new parameters are added to search variables which are R_B, and s, slider range. With five variables it is difficult to visualize the character of the optimum solutions and to model it. A numerical search method can also be applied to find the optimum results again. Instead of the no slider constraint case, the inverse kinematic solution has slider constraints this time.

The orientation workspace with slider constraints at a specified position for a configuration is shown in Figure 6.12.

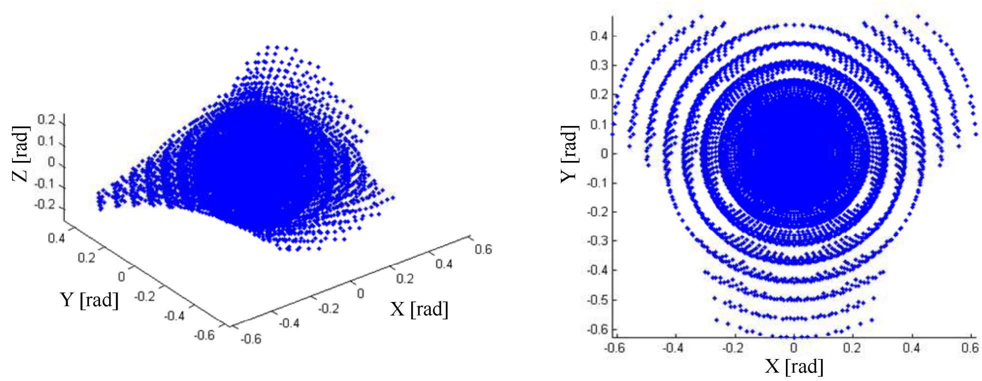

Figure 6.12. Visualization of the orientation workspace with slider constraints

It is observed that the boundary of the orientation workspace is smaller, as expected. The feature of the object is an excellent sphere with three wings, which represents the symmetry of $2/3\pi$. It means that the z component of the orientation workspace has to be considered this time. Therefore a spherical fit method should be applied instead of circle fit.

A numerical search is performed to analyze the optimality of the dimensions with various combinations of the parameters. Δz versus the radius of the sphere is implemented in Figure 6.13,Figure 6.14 and Figure 6.15, with various L, ρ, and R_B values.

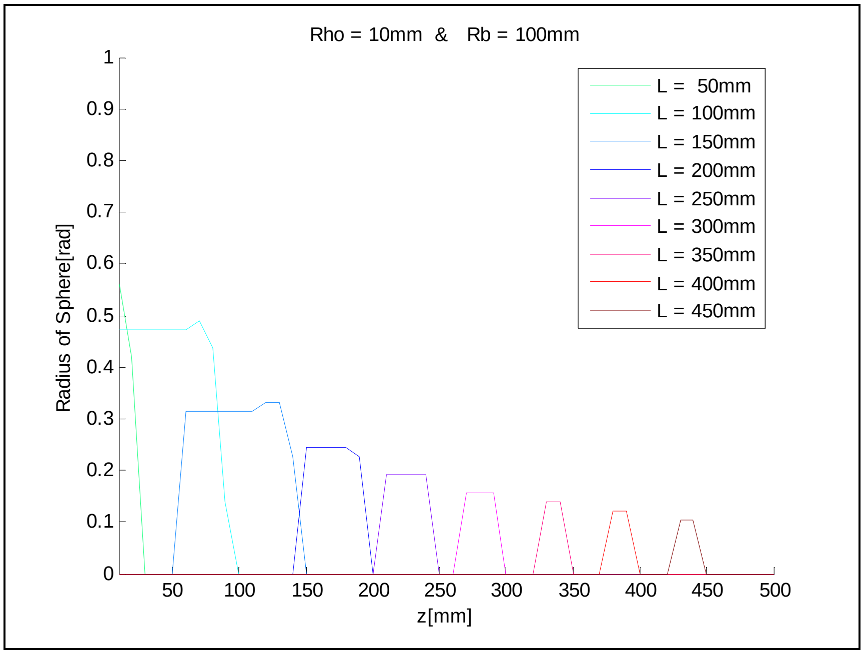

Figure 6.13. Investigation of the orientation workspace, ρ=10 mm, R_B=100 mm

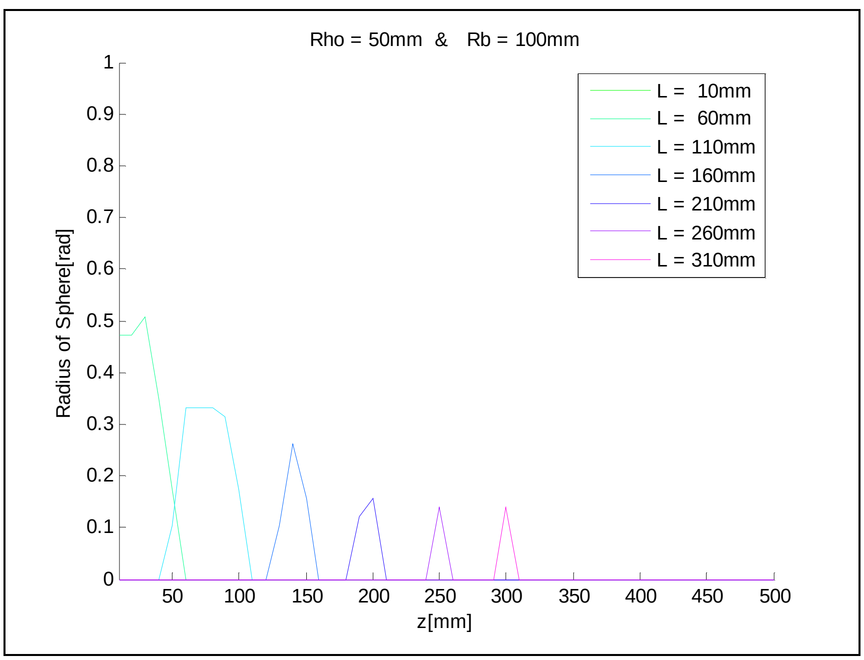

Figure 6.14. Investigation of the orientation workspace, ρ=50 mm, R_B=100 mm

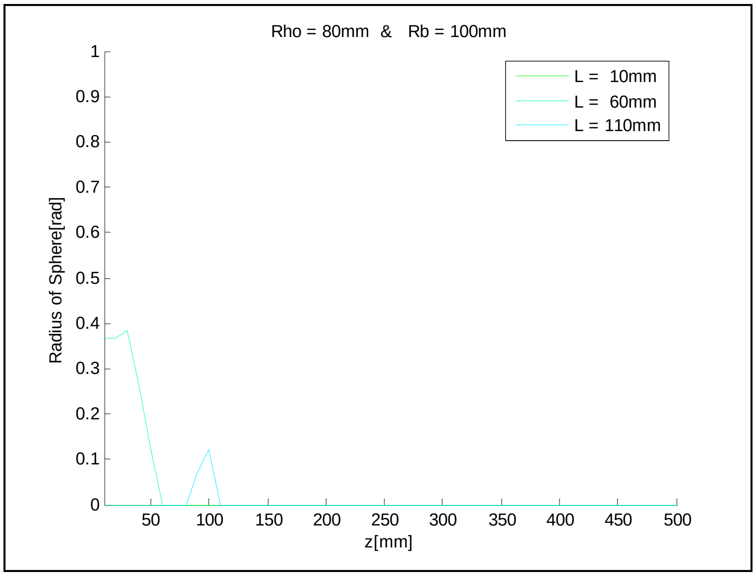

Figure 6.15. Investigation of the orientation workspace, ρ=80 mm, R_B=100 mm

In Figure 6.13, when L increases R and Δz decreases. Selection of the minimum L gives the maximum R. In Figure 6.14 and Figure 6.15, it is observed that when ρ increases the range of L changes, due to kinematic solution existence. Furthermore, any L value in these sets cannot achieve the R that is achieved in Figure 6.13 with L=100 mm.

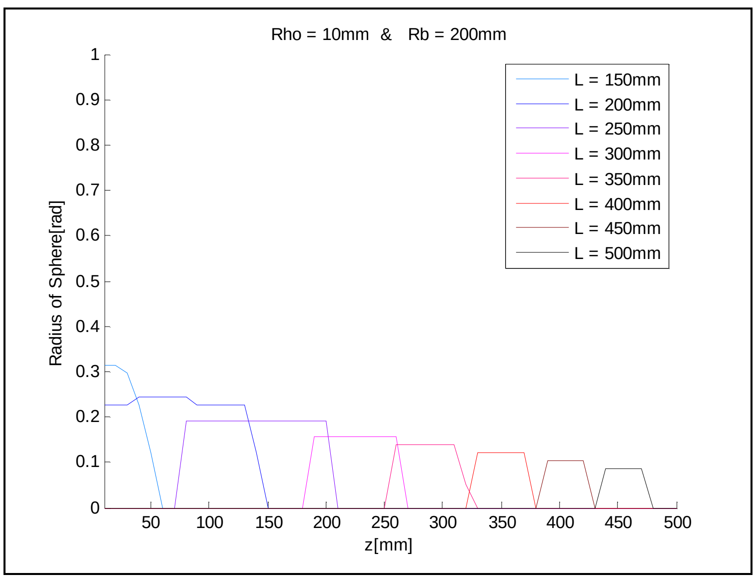

Figure 6.16. Investigation of the orientation workspace, ρ=10 mm, R_B=200 mm

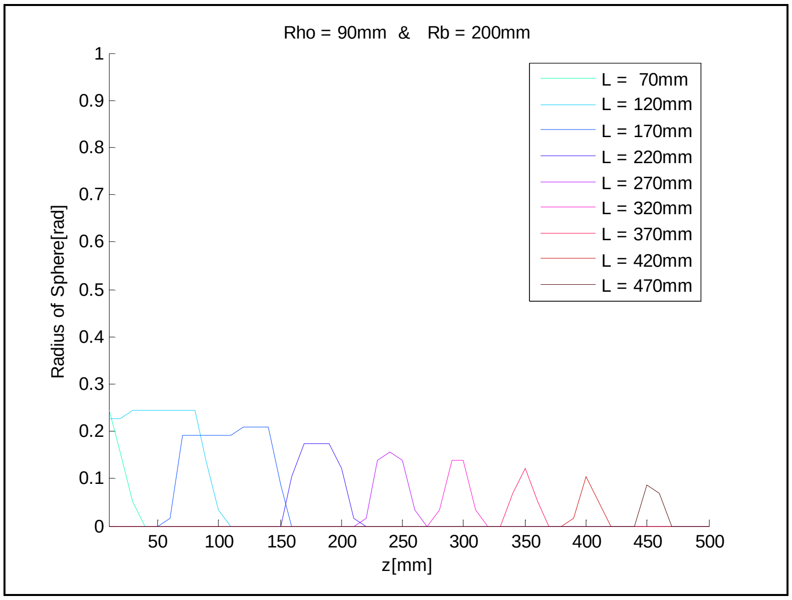

Figure 6.17. Investigation of the orientation workspace, ρ=90 mm, R_B=200 mm

In Figure 6.16 and Figure 6.17, the effect of the R_B is studied. Similar to the group of Figure 6.13, Figure 6.14 and Figure 6.15, it is observed that when ρ increases, the achievable R decreases. When R_B is increased the achievable Δz increases however R decreases. In micromachining process, the translational range of the z was determined as 10 mm. This specification is satisfied when R_B is 100mm. Therefore, R_B has to be selected as small as possible, in order to increase R and it is clear that smaller ρ values give better results.

The minimum values for those parameters actually depend on manufacturability. The smallest value for ρ is assumed to be 50 mm when the connections of revolute joints are considered. The smallest value for L is assumed to be 100 mm. The smallest value for R_B can be decided by the slider dimensions. The smallest radius where any slider would not collide to each other is computed as 237.5 mm, shown in Figure 6.18.

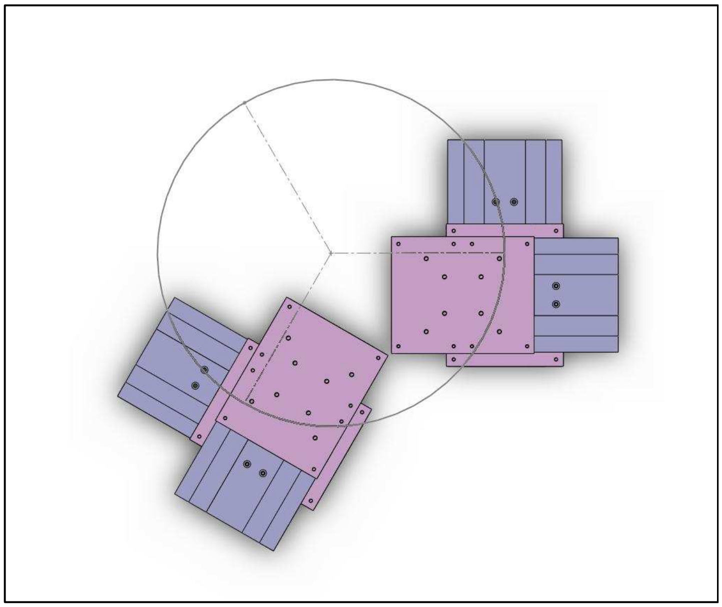

Figure 6.18. Calculation of the smallest R_B

Another search with a constant R_B and ρ starting from 50 mm, is conducted with a smaller stepsizes of variables, illustrated in Figure 6.19.

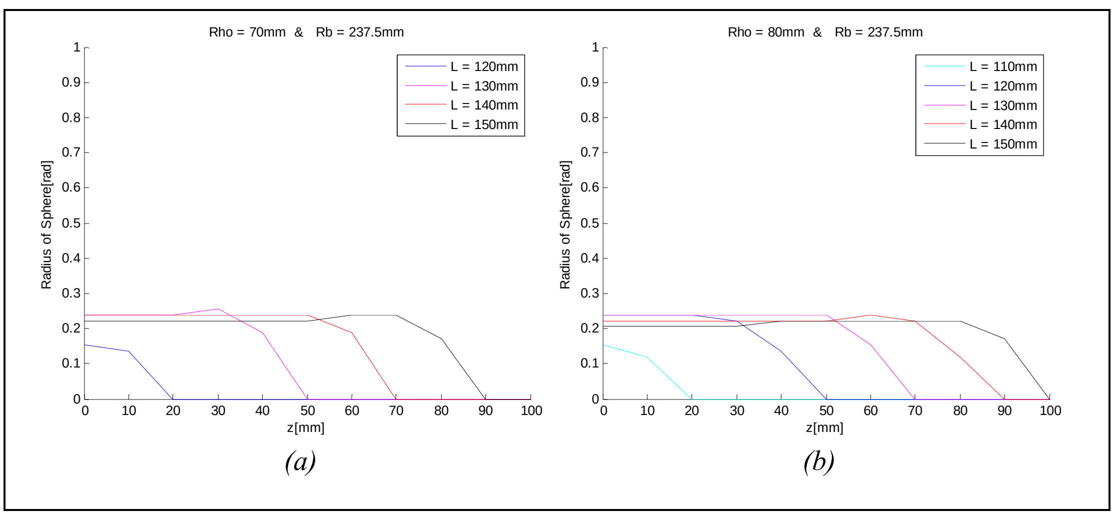

Figure 6.19. Investigation of optimum values for the minimum R_B (a) ρ=70 mm (b) ρ=80 mm

According to the results the optimal values are found as; L is 130 mm, ρ is 80 mm, within a range of $0\ mm \leq z \leq 50\ mm$ where R is equal to 0.2443 rad.

Before this study, the dimensions of the manipulator were chosen: L as 500 mm, ρ as 400 mm, and R_B as 600 mm. According to these values, R is found as 0.06 radian at maximum where Δz satisfies the micromachining requirements, shown in Figure 6.20.

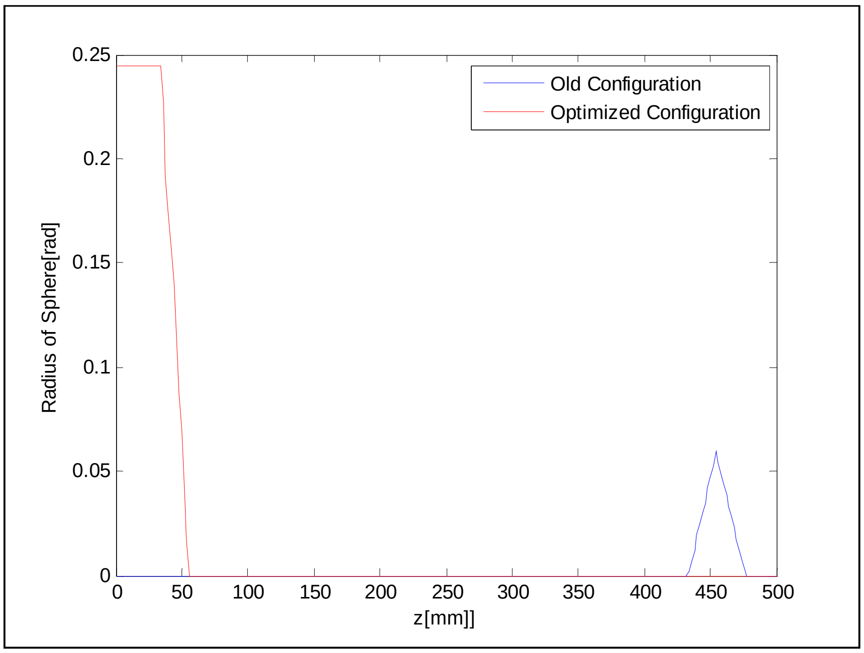

Figure 6.20. Evolution of theYPM

In conclusion, the orientation capability of the manipulator is increased to 0.2443 rad, with a 330% rise.

7. CONCLUSION

In this study, kinematic composition of the YPM is defined and the components are studied extensively. The kinematic components are introduced and their specifications are mentioned. After the definition of the physical constraints, the topology of the YPM is investigated, and the kinematic diagram is illustrated. Mobility of the YPM is evaluated as six, using Gruebler's Equation.

The kinematic relations of the YPM are defined and the inverse kinematic solution is explored. At this moment, multiple solutions of YPM are investigated and analyzed. A MATLAB algorithm is developed to solve the slider positions for a given platform position and orientation.

Definition of the workspace is stated and the optimum workspace of YPM is defined the as maximal workspace. The maximal workspace aims the largest translational workspace with maximal orientations. According to the concept of maximal workspace, representations of translation and orientation workspaces are studied. Dimensional configurations only affect the z direction of the translational workspace. It is stated that the optimization of the translational workspace is reduced to one dimensional problem. In order to get a proper calculation of the orientation workspace size, three representations of a rotation matrix are considered. After the definitions of these representations, visualization of them is discussed to determine the best. XYZ Fixed Angles is concluded to be the best representation. The feature of this representation is reasonable and the kinematic circuits in this representation are definite. However some orientations repeat themselves while the full range of representation parameters are swept. In order to avoid the repetition of the orientations, Equivalent Angle-Axis Representation can be used to form the rotation matrices. The ranges of rotation matrix parameters in XYZ Fixed Angles are explored by the help of Equivalent Angle-Axis Representation. The orientation workspace is reduced to two dimensional problem where z direction has no effect. Therefore three dimensional size calculation is simplified to area calculation.

When the orientation workspaces of different configurations at a constant position are considered, it is observed that the kinematic circuits get connected for specific ratios. Furthermore, the appearances of the kinematic circuits at those instants are absolutely unique. The critical leg length concept is defined and the critical lengths are investigated for various configurations. The relationship of the search parameters are found as

$$L_{critical} = \rho + z \qquad (6.1)$$

The default orientation and its neighbors form the most important region in the orientation workspace. A circle fitting method is developed to compare the sizes of the circuits.

First optimization is performed without slider limitations. The optimum configuration table is obtained for a given Δz. By using circle fitting method, the optimum configuration for Δz=200 mm is determined as $\rho = 10\text{ mm},\ L = 409.2306\text{ mm}$.

In the second optimization, slider limitations are considered. Therefore, the feature of the orientation workspace is found as a sphere with three symmetric wings. Instead of circle fitting method, a sphere fitting method is applied to measure the orientation capability. In this case the orientation workspace is a three dimensional volume and maximal sphere radius indicates the maximal orientation workspace. Another numerical optimization is performed with various configurations. In this optimization, there are two more variables which are R_B and s, compared to no slider limitation case. According to results, it is observed that the minimum R_B and smaller ρ are required to optimize the workspace. Therefore, the manufacturability of the components is considered and the optimum result with YPM sliders is found as; L is 130 mm, ρ is 80 mm and R_B is 237.5 mm. This configuration gives 0.2443 rad rotations about all the three axes.

Before this study, the dimensions of the manipulator were taken as; L is 500 mm, ρ is 400 mm, and R_B is 600 mm. When this configuration is compared with the optimized one, a 330% increase in orientation capability is achieved.

8. REFERENCES

1. "Micro Drilling Examples", Inc. HSR Business to Business. http://www.makino.com/. [Online] 2008.

2. Bamberger, Hagay, Shoham and Moshe, "A New Configuration of a Six Degrees-of-Freedom", Proceedings of the 2004 IEEE International Conference on Robotics & Automation, New Orleans, 2004.

3. Fox, R. L. and Gupta, K. C, "Optimization technology as applied to mechanism design", J. Eng. Industry, pp. 657-663, May 1973.

4. Hollerbach, J. H., "Optimum kinematic design of a seven degree of freedom manipulator", Proc. Robotics Res., 2nd Int. Symp, Cambridge, 1985.

5. Merlet, J. P. and INRIA, Daney, D., "Dimensional Synthesis of Parallel Robots with a Guaranteed Given Accuracy over a Specific Workspace", International Conference on Robotics and Automation, Proceedings of the 2005 IEEE, Barcelona, 2005.

6. Ng, C. C., Ong, S. K. and Nee, A. Y. C, "Design and development of 3–DOF modular micro parallel kinematic manipulator", Springer-Verlag, London, 2006.

7. Liua, X. C., "Optimum design of 3-DOF spherical parallel manipulators with respect to the conditioning and stiffness indices", Mechanism and Machine Theory, Vol. 35, pp. 1257-1267, 2000.

8. Dafaoui, H. T. and El-Mouloudi, E. A., "Analysis and Design of a Six-DOF Parallel Manipulator, Modeling, Singular Configurations, and Workspace", IEEE TRANSACTIONS ON ROBOTICS AND AUTOMATION, Vol. 14, 1998.

9. Merlet, J. P., "Determination of the optimal geometry of modular parallel robots", Proceedings of the 2003 IEEE Internatioal Conference on Robotics & Automation, 2003.

10. Kim, L. V., "Design Optimization of a Cartesian Parallel Manipulator", Journal of Mechanical Design, Vol. 125, March 2003.

11. Stoughton, R. T., "A Modified Stewart Platform Manipulator with Improved Dexterity", IEEE TRANSACTIONS ON ROBOTICS AND AUTOMATION, Vol. 9, 1993.

12. Zhaoa, H. K and Jing, S., "Optimizing the kinematic chains for a spatial parallel manipulator via searching the desired dexterous workspace", Robotics and Computer-Integrated Manufacturing, Vol. 23, pp. 38–46, 2007.

13. Lou, Y. L. and Yunjiang, L. G., "Randomized Optimal Design of Parallel Manipulators", IEEE Transactions On Automation Science And Engineering, Vol. 10, 2007.

14. Feng, G. and Xin, X. C., "The relationships between the shapes of the workspaces and the link lengths of 3-DOF symmetrical planar parallel manipulators", Mechanism and Machine Theory, Vol. 36, pp. 205-220, 2001.

15. Arakelian, V. and Se´bastien, G. V., "Increase of singularity-free zones in the workspace of parallel manipulators using mechanisms of variable structure", Mechanism and Machine Theory, Vol. 43, pp. 1129–1140, 2008.

16. Liu, X. J., "Optimum design of the 5R symmetrical parallel manipulator with a surrounded and good-condition workspace", Robotics and Autonomous Systems, Vol. 54, pp. 221–233, 2006.

17. Majid, M. Z. A. and Huang, Z., "Workspace Analysis of a Six-Degrees of Freedom, Three-Prismatic-Prismatic-Spheric-Revolute Parallel Manipulator", Int J Adv Manuf Technol Springer-Verlag London Limited, Vol. 16, pp. 441–449, 2000.

18. Wang, X. B., "Topology of serial and parallel manipulators and topological diagrams", Mechanism and Machine Theory, Vol. 43, pp. 754-770, 2008.

19. "Aerotech ABL1000 Air Bearing Stage", Aerotech Inc., 2005, http://www.aerotech.com/products/airbearing/abl1000.htm, [Online].

20. "Rodrigues Parameters Representation", Wikipedia, the free encyclopedia, http://en.wikipedia.org/wiki/Rotation_representation_%28mathematics%29.

21. Craig, John J., Introduction to Robotics, Mechanics and Control 3, Pearson Prentice Hall, 0-13-123629-6, 2005.

22. Stoughton, K. F., Robert, S. and Arai, T., "A Modified Stewart Platform Manipulator with Improved Dexterity", IEEE TRANSACTIONS ON ROBOTICS AND AUTOMATION, Vol. 9, 1993.

23. Merlet, J. P., "Determination of the optimal geometry of modular parallel robots", Proceedings of the 2003 IEEE Internatioal Conference on Robotics & Automation, 2003.

24. Kim, H. S. and Tsai, L., W., "Design Optimization of a Cartesian Parallel Manipulator", Journal of Mechanical Design, Vol. 125, March 2003.

25. Markine, V.L., "Optimization of a manipulator for a flight simulator". http://www.brad.ac.uk/staff/vtoropov/burgeon/b_flsim.htm. [Online].

26. Arthur G., Sandor, G. N. and Kota, S., Mechanism Design, Prentice Hill, pp. 21, Vol. 1, 2001.

27. Kramer, G., "A. Solving geometric constraint systems", MIT Proceedings, p. 11. 0262111640, 1992.